Mycoscience VOL.65 (2024) 49–67

Mycoscience

An open access journal for general mycology

The Mycological Society of Japan

Full paper

Amanita satotamagotake sp. nov., a cryptic species formerly included in *Amanita caesareoides*

Miyuki Kodaira[a], Wataru Aoki[b], Naoki Endo[c], Daisuke Sakuma[d], Eiji Hadano[e], Atsuko Hadano[e], Yasushi Hashimoto[f], Seiki Gisusi[g], Kohei Yamamoto[h], Ryo Sugawara[i], Masaki Fukuda[a, b, i], Akiyoshi Yamada[a, b, i, j*]

[a] *Department of Agriculture and Life Science, Graduate School of Science and Technology, Shinshu University, 8304, Minami-minowa, Kami-ina, Nagano, 399-4598, Japan*

[b] *Department of Science and Technology, Graduate School of Medicine, Science and Technology, Shinshu University, 8304, Minami-minowa, Kami-ina, Nagano, 399-4598, Japan*

[c] *Faculty of Agriculture, Tottori University, 4-101, Koyama-cho Minami, Tottori, 680-8553, Japan*

[d] *Osaka Museum of Natural History, 1-23, Nagai-koen, Higashi-sumiyoshi-ku, Osaka, 546-0034, Japan.*

[e] *1-1-36, Ryougo, Oita, 870-0883, Japan.*

[f] *Department of Agro-environmental Science, Obihiro University of Agriculture and Veterinary Medicine, 2-1, Inada-cho, Obihiro, Hokkaido, 080-8555, Japan*

[g] *Forest Products Research Institute, Hokkaido Research Organization, 1-10, Nishikagura, Asahikawa, Hokkaido 071-0198, Japan*

[h] *Tochigi Prefectural Museum, 2-2, Mutsumi-cho, Utsunomiya, Tochigi, 320-0865, Japan*

[i] *Faculty of Agriculture, Shinshu University, 8304, Minami-minowa, Kami-ina, Nagano, 399-4598, Japan*

[j] *Institute for Mountain Science, Shinshu University, 8304, Minami-minowa, Kami-ina, Nagano, 399-4598, Japan*

ABSTRACT

We evaluated the inclusion of a cryptic species in a Japanese *Amanita caesareoides* population. We sampled *A. caesareoides* specimens under various vegetation and climate conditions, and then conducted phylogenetic analyses on sequences from seven loci. The *A. caesareoides* specimens showed two distinct groups, except when the ITS phylogeny was considered. These two phylogroups showed different distributions: subalpine–cool temperate and temperate–subtropical areas. Although these two phylogroups overlapped in terms of basidiospore size, the latter tended to exhibit smaller basidiospores. In addition, only the former showed mycelial growth on nutrient agar. Based on these phylo-morpho-ecophysiological characteristics, we separated the specimens labeled with the name *A. caesareoides* into two species. As the lectotype of *A. caesareoides* showed similarity to the former by DNA analysis, the latter was described as a new species, namely *A. satotamagotake*. Based on the geographic patterns of the two species, *A. satotamagotake* may have invaded the natural habit of *A. caesareoides* because of global warming.

Keywords: biogeography, Caesar's mushroom, ectomycorrhizal association, multi-locus concatenate phylogenetic analyses, speciation

Article history: Received 14 March 2023, Revised 1 December 2023, Accepted 4 December 2023, Available online 31 March 2024.

1. Introduction

Amanita caesareoides Lj.N. Vassiljeva, belonging to the section *Caesareae*, is associated with *Pinaceae* and *Fagaceae* trees as an ectomycorrhizal symbiont (Endo, 2015; Endo et al., 2013). Several species in the sect. *Caesareae* ("Caesar's mushrooms") are edible mushrooms and are consumed globally. The sect. *Caesareae* is estimated to have originated around 60 Mya (Paleocene) in the Africa, and then expanded to Europe, Australia, and North and Central America through southwest of Laurasia (present southeast Asia) (Sánchez-Ramírez et al., 2015a). In Japan and the surrounding Far East Asian region, the reddish-pileus Caesar's mushrooms, represented by *A. caesareoides*, are estimated to have expanded from the ancestral clade around 8–6 Mya (late Miocene; Tortonian–Messinian) (Sánchez-Ramírez et al., 2015a).

Amanita caesareoides was first described from the Kamchatka Peninsula, Russia (Vassiljeva, 1950) but treated as *A. caesarea* (Scop.) Pers. or *A. hemibapha* (Berk. & Broome) Sacc. in East Asia (Cho et al., 2015; Endo et al., 2016; Yang, 2005; Zhang et al., 2004). In Japan, *A. caesareoides* was initially identified as *A. caesarea* by Hennings (1900) with the common name "Oobenitake," which means "large crimson mushroom" in Japanese (Matsumura, 1904; Shirai, 1905; Shirai & Hennings, 1899). The specimen identified as *A. caesarea* by Hennings (1900) was collected by Mitsutaro Shirai in 1894 in a *Quercus crispula* forest under a cool-temperate climate at the lakeside of Chuzenji-ko, Nikko, Tochigi Prefecture; its external morphology was illustrated in color (Shirai & Hennings, 1899). Kawamura (1913) described Japanese *A. caesarea* with a color

* Corresponding author.
E-mail address: akiyosh@shinshu-u.ac.jp

drawing of basidiomata, a description of its local name "Tamagotake" (egg mushroom in Japanese), and its consumption by the local inhabitants. Subsequently, Tamagotake was accepted as the Japanese common name of *A. caesarea* (Shirai & Miyake, 1917; Yasuda, 1920). Kawamura (1954) suggested that Japanese *A. caesarea* includes three varieties distinguished by pileal color: yellow, reddish orange (vermilion), and deep red (crimson). Yasuda (1920) described the microscopic features of Japanese *A. caesarea*, which corresponds to the yellowish-pileus type reported by Kawamura (1954). The *A. caesarea* specimen of Yasuda (1920) was sampled in 1919 in Kiso-fukushima, Nagano Prefecture, presumably under an intermediate-temperate climate. The yellowish-pileus type of *A. caesarea* reported by Kawamura (1954) was sampled on Jul 13, 1928, in Matsudo, Chiba Prefecture, under a warm-temperate climate. The crimson-pileus type of *A. caesarea* corresponds to the specimen of Kawamura (1913), which was sampled on Oct 30, 1910, in southwest Iizuna (at the foot of Mt. Reisenji-yama), Nagano Prefecture (Kawamura, 1930, 1954), presumably under a cool-temperate climate. Although the sampling site of the other vermilion-pileus type of *A. caesarea* reported by Kawamura (1954) was not described, a corresponding specimen was sampled in Oct 1930, in Sanbu, Chiba Prefecture (warm-temperate climate) (Kawamura, 1931). Hongo (1975) identified the reddish-pileus type(s) of Japanese *A. caesarea* as *A. hemibapha* subsp. *hemibapha* (Berk. & Broome) Sacc. and newly reported a brown-pileus type (newly named Chatamagotake) as *A. hemibapha* subsp. *similis* (Boedijn) Corner & Bas, and Hongo (1982) identified the yellowish-pileus type (newly named Kitamagotake) as *A. hemibapha* subsp. *javanica* Corner & Bas. Hongo (1982), and Imazeki and Hongo (1987) regarded Japanese *A. hemibapha* as conspecific to *A. caesareoides*. However, Hongo (1975, 1982) and Imazeki and Hongo (1987) did not observe type specimens of *A. hemibapha* or *A. caesareoides*. Hongo (1975) inspected an *A. hemibapha* specimen sampled in Nango-Imodani, Otsu, Shiga Prefecture, under a warm-temperate climate; this specimen may correspond to the vermilion-pileus type of *A. caesarea* reported by Kawamura (1954) (Table 1).

Oda et al. (1999) raised *A. hemibapha* subsp. *javanica* to species rank as *A. javanica* (Coner & Bas) T. Oda, C. Tanaka & Tsuda, based on a phylogenetic analysis of the internal transcribed spacer (ITS) region of the nuclear rDNA operon (nuc rDNA). However, they did not examine the type specimens of *A. hemibapha* or *A. hemibapha* subsp. *javanica* (Endo et al., 2016, 2017). Japanese *A. hemibapha* subsp. *javanica* was recently distinguished from the type specimen of *A. hemibapha* subsp. *javanica* (distributed in the south and southeast Asian regions) and newly described as *A. kitamagotake* N. Endo & A. Yamada (Endo et al., 2017). The Japanese reddish-pileus type(s) *A. hemibapha* subsp. *hemibapha* was compared with its Asian relatives, including the lectotype of *A. caesareoides*, and identified as *A. caesareoides,* based on morphological characteristics and a phylogenetic analysis of the nuc rDNA ITS region (Endo, 2015; Endo et al., 2013, 2016). Notably, Japanese *A. caesareoides* exhibits variations in spore size and culture characteristics, suggesting two ecological groups: subalpine–cool-temperate and warm-temperate–subtropical (Endo, 2015). This is reminiscent of the different color types of Tamagotake (i.e., vermilion- and crimson-pileus types) described by Kawamura (1954). Therefore, we hypothesized that the Japanese *A. caesareoides* population consists of two independent species. To test this hypothesis, we conducted phylogenetic analyses of five nuclear DNA loci, i.e., the ITS and intergenic spacer 1 (IGS1) regions of nuc rDNA, the genes encoding beta-tubulin (*β-TUB*), RNA polymerase II subunit 2 (*RPB2*), and translation elongation factor 1α (*TEF1*), and two mitochondrial DNA loci, i.e., ATPase subunit 6 (*ATP6*) and cytochrome c oxidase subunit 3 (*COX3*), and morphological observations of the Japanese *A. caesareoides* and other species in sect. *Caesareae*. In addition, we established cultures of *A. caesareoides* and performed comparisons of its colony morphology and vegetative mycelial

Table 1. Taxonomic history of Japanese Caesar's mushrooms, *Tamagotake* and its related species.

Reference	Adopted Latin name and Japanese common name in the quotation marks			
Shirai & Hennings (1899), Hennings (1900)	*Amanita caesarea* (red pileus) "Oobenitake"			
↓				
Kawamura (1913)	*Amanita caesarea* (red pileus) "Tamagotake"			
↓				
Yasuda (1920), Kawamura (1930, 1931)	*Amanita caesarea* (red pileus) "Tamagotake"		*A. caesarea* (yellow pileus) "Tamagotake"	
↓	↓		↓	
Kawamura (1954)	*A. caesarea*, crimson-pileus type "Tamagotake"	*A. caesarea*, vermillion-pileus type "Tamagotake"	*A. caesarea*, yellow-pileus type "Tamagotake"	
↓	↓			
Hongo (1975)	*A. hemibapha* subsp. *hemibapha* "Tamagotake"		↓	*A. hemibapha* subsp. *similis* (brown pileus) "Chatamagotake"
↓				↓
Hongo (1982)	*A. hemibapha* subsp. *hemibapha* (= *A. caesareoides*) "Tamagotake"		*A. hemibapha* subsp. *javanica* "Kitamagotake"	*A. hemibapha* subsp. *similis* "Chatamagotake"
↓			↓	↓
Oda et al. (1999)	*A. hemibapha* "Tamagotake"		*A. javanica* "Kitamagotake"	*A. similis* "Chatamagotake"
↓				
Endo et al. (2013, 2016), Endo (2015)	*A. caesareoides* "Tamagotake"		↓	↓
↓				
Endo et al. (2017)	*A. caesareoides* "Tamagotake"		*A. kitamagotake* sp. nov. "Kitamagotake"	*A. chatamagotake* sp. nov. "Chatamagotake"

structure. Based on the resulting data, we describe a new *Amanita* species that was cryptic to *A. caesareoides*. As the taxonomic positions of these two closely related species suggested that they have distinct geographic distributions, we discuss their ecological significance in relation to land use in Japan and climate change.

2. Materials and Methods

2.1. Sampling and morphological observation of Tamagotake

Specimens of *A. caesareoides* were collected in various forests in Japan between 2008 and 2020 (Table 2; Fig. 1). The following macroscopic characteristics of basidiomata were recorded: pileal color, shape, and diam; lamella width and color; stipe length, width, and surface ornamentation; and volval shape, width, length, and color. Young, fresh basidiomata were collected for tissue isolation (see below). Subsequently, basidiomata were freeze-dried, oven-dried at 60 °C overnight, and stored in the laboratory as dried specimens. Where necessary, specimens were deposited in the National Museum of Nature and Science (TNS), Japan. The warmth index (WI) (Kira, 1948) of each sampling site was estimated to characterize the vegetation zone and habitat properties: 15–45, subarctic (subalpine) evergreen coniferous forests; 45–85, cool-temperate deciduous broad-leaved forests; ~85, intermediate-temperate deciduous broad-leaved forests; 85–180, warm-temperate evergreen broad-leaved forests; and 180–240, subtropical evergreen broad-leaved forests (Supplementary Table S1). The coldness index (CI) (Kira, 1948) and mean annual temperature (MAT) were also estimated for each sampling site. These indices were calculated based on AMEDAS data (Japan Meteorological Agency; http://www.jma.go.jp/jma/index.html) of the one to three points nearest each sampling site, using a lapse rate of 0.55 °C/100 m around the Japanese Archipelago (Yoshino, 1986).

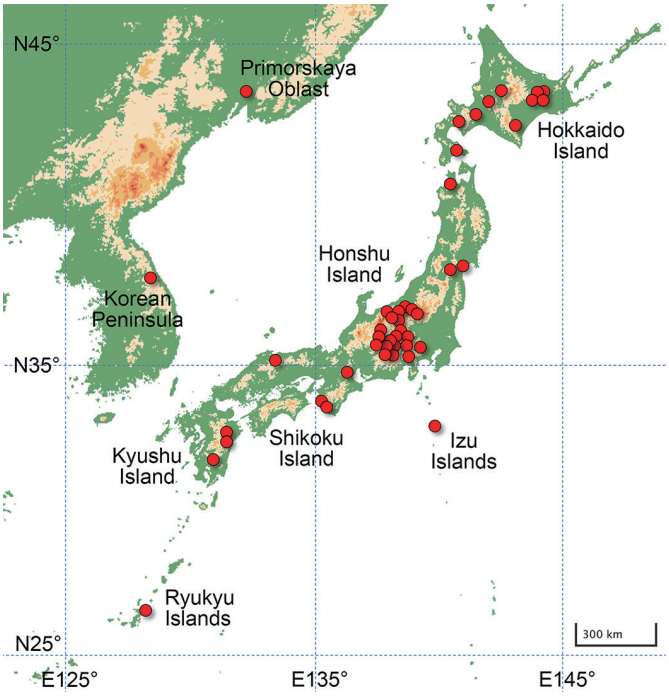

Fig. 1 – Sampling sites of *Amanita caesareoides* specimens in the Japanese Islands and surrounding areas. Red circles represent sampling sites from some of which several specimens were sampled on different dates from under different tree species (Table 2). The geographic map was manually constructed on the website of the Geospatial Information Authority of Japan (https://maps.gsi.go.jp/vector/). Green, < 500 m above sea level; cream to dark brown, 500 to > 2500 m above sea level at 500 m intervals.

2.2. Tamagotake tissue isolation

As the culture characteristics of Japanese *A. caesareoides* differ between specimens sampled from subalpine–cool temperate and warm temperate forests (Endo, 2015), we subjected young basidiomata to tissue isolation using the method reported by Endo et al. (2013) with minor modification. The basidiomata surface was wiped with absorbent cotton soaked in 70% ethanol; pileus inner tissue was axenically cut into several 2 × 2-mm mycelial pieces using a scalpel, then inoculated on modified Norkran's C (MNC) agar (Yamada & Katsuya, 1995). The specimens were incubated for 4 mo in an air-conditioned room (~20 °C–25 °C), and mycelium growth was observed under a stereoscopic microscope (Stemi 2000-C; Carl Zeiss AG, Jena, Germany). Mycelia and colonies were also observed under a differential interference contrast microscope (AXIO Imager A1; Carl Zeiss AG) and hyphal width was measured.

2.3. Microscopic observation

Small pieces of dried specimens were rehydrated in 70% ethanol for 1 min, transferred to distilled water to fully rehydrate mycelia (~1–2 h), and mounted with 100% lactic acid on a glass slide. If necessary, basidia were stained with acid fuchsin. Hyphae and basidiospores were observed under a differential interference contrast microscope with a 40× or 100× oil-immersion objective lens (Plan NEO FLUAR), then photographed. The sizes of 50 basidiospores, 30 basidia, 10 sterigmata, and 10 cheilocystidia-like terminally inflated hyphae at the lamella edge were measured for each specimen. Pileipellis, tramal tissue of the pileus, stipitipellis, inner tissue of the stipe, annulus, and volval tissue were observed in several selected specimens.

2.4. DNA analysis

Genomic DNA was extracted from dried specimens of *A. caesareoides*, *A. caesarea*, *A. kitamagotake* and *A. chatamagotake* N. Endo & A. Yamada by the cetyltrimethylammonium bromide method (Endo et al., 2016; Gardes & Bruns, 1993) with minor modifications. We performed DNA analyses of the ITS and IGS1 regions of nuc rDNA, *β-TUB*, *RPB2*, and *TEF1*, and the mitochondrial *ATP6* and *COX3* genes. The primers used for PCR amplification are shown in Table 3. Several primers were newly designed for DNA amplification from old specimens (i.e., *A. caesareoides* LE203026 [lectotype; Vassiljeva, 1950] and Hongo 5297 [Hongo, 1975]). PCR amplification was conducted using Dream Taq DNA polymerase (Thermo Fisher Scientific, Waltham, MA, USA) or Tks Gflex™ DNA Polymerase (TaKaRa, Kusatsu, Japan) and ProFlex 3 × 32-well PCR System (Applied Biosystems, Foster City, CA, USA) or GeneAmp®PCR System 2700 (Applied Biosystems). First-round PCR for ITS, IGS1, *β-TUB*, *ATP6*, and *COX3* was conducted with an initial denaturation step at 95 °C for 3 min followed by 40 cycles of denaturation at 95 °C for 30 s, annealing at 52 °C for 30 s, and extension at 72 °C for 1 min (ITS, *β-TUB*, *COX3*, *ATP6*) or 90 s (for IGS1), with a final extension step at 72 °C for 7 min (ITS, *β-TUB*, *COX3*, *ATP6*) or 10 min (IGS1). To amplify *TEF1*, touchdown PCR was conducted with an initial denaturation step at 95 °C for 3 min followed by 40 cycles of denaturation at 95 °C for 15 s, annealing at 65 °C decreasing by 1 °C per cycle (cycles 1–10) or 52 °C (cycles 12–40), and extension at 72 °C for 1.5 min, with a and final extension step at 72 °C for 10 min. To amplify *TEF1* from the Hongo 5297 specimen, PCR was conducted using the *tef1*-AcoidesF/*tef1*-

Table 2. Specimens examined in the present study.

Species and specimens		Sampling			
		Date (Y.M.D)	Site		
			Locality in Japan [b]	Altitude (m)	Canopy vegetation [c]
Amanita caesareoides [a]					
AC-59-1	A	2018.8.1	Kamisato, Tsubetsu, Hokkaido	406	As
AC-60-2	A	2018.8.1	Lake side of Chimikeppu-ko, Tsubetsu, Hokkaido	309	As
S-319	A	2012.9.23	Lake side of Akan-ko, Kushiro, Hokkaido	430	ND
AC-58-2	A	2018.7.31	Onneto, Ashoro, Hokkaido	638	As
As2-2 (= TNS-F-61971)	A	2009.8.10	Kaguraoka-kouen, Asahikawa, Hokkaido	118	As
AC-51	A	2017.9.20	Iwanai-senkyo, Obihiro, Hokkaido	241	Be
AY-2150918-011	A	2015.9.18	Bibai, Hokkaido, Japan	55	Pa
S-257 (= TNS-F-61979)	B	2011.9.9	Atsubetsu, Sapporo, Hokkaido	35	Qc, Bp
S-320	B	2012.9.25	Atsubetsu, Sapporo, Hokkaido	35	Qc, Bp
S-259 (= TNS-F-61980)	A	2011.9.9	Makkari, Hokkaido	207	As
AC-76	A	2018.9.11	Lake side of Oo-numa, Nanae, Hokkaido	130	Fc, Qc
AC-24	B	2017.7.17	Goshogawara, Aomori	74	Bp
AC-36 (TNS-F-82293)	B	2017.8.14	Shichigahama, Miyagi	37	Af
AC-62	A	2018.8.23	Mt. Sanpou-koujin-san, Yamagata, Yamagata	1607	Am, Pp
AY-2130927-003	A	2013.9.27	Lake side of Suga-numa, Katashina, Gunma	1735	Av, Be, Bp
AC-37-2	B	2017.8.21	Mikuni-touge Pass, Minakami, Gunma	1200	Fc
AC-11	B	2016.8.15	Mt. Atema-yama, Tookamachi, Niigata	750	Fc
AC-40-1	A	2017.8.29	Sasagamine, Myoko, Niigata	1317	Fc, Qc
AC-41-2	B	2017.8.30	Mt. Madarao-san, Myoko, Niigata	949	Fc
AC-41-1		2017.8.30	Mt. Madarao-san, Iiyama, Nagano	914	Fc
AC-72-1	A	2018.10.8	Mt. Madarao-san, Iiyama, Nagano	933	Qc
AC-72-2	A	2018.10.8	Mt. Madarao-san, Iiyama, Nagano	933	Qc
AC-32	B	2017.8.6	Otari, Nagano	930	Fc
AC-70-1	B	2018.9.19	Lake side of Nojiri-ko, Shinano, Nagano	684	Qs, Qc, Fc
AC-70-5	B	2018.9.19	Lake side of Nojiri-ko, Shinano, Nagano	684	Qc
S-292 (= TNS-F-61981)	A	2012.6.23	Lake side of Reisenji-ko, Iizuna, Nagano	840	Pa
AC-1		2016.7.17	Lake side of Reisenji-ko, Iizuna, Nagano	845	ND
AC-66-1	A	2018.9.12	Lake side of Reisenji-ko, Iizuna, Nagano	841	Pa
AC-66-10	B	2018.9.12	Lake side of Reisenji-ko, Iizuna, Nagano	847	Pa
AC-66-11	B	2018.9.12	Lake side of Reisenji-ko, Iizuna, Nagano	847	Pa
AC-3	B	2016.7.16	Ooyachi-shitsugen wetland, Nagano, Nagano	1040	Pd, Lk, Qs, Bp
AC-2	B	2016.7.16	Ichinotorii, Nagano, Nagano	1162	Pd
AC-67-1	A	2018.9.12	Togakushi, Nagano, Nagano	1170	Qc
S-317	A	2012.8.15	Sugadaira, Ueda, Nagano	1350	ND
AC-44	A	2017.9.4	Kamikouchi, Matsumoto, Nagano	1497	Td
S-230 (= TNS-F-61976)	A	2011.7.18	Mt. Norikura-dake, Matsumoto, Nagano	1455	Qc
S-231	A	2011.7.18	Mt. Norikura-dake, Matsumoto, Nagano	1455	Qc
AC-49	A	2017.9.13	Mt. Norikura-dake, Matsumoto, Nagano	1444	Qc
AC-50	A	2017.9.14	Mt. Norikura-dake, Matsumoto, Nagano	1613	Qc, Fc
S-242	B	2011.7.18	Daira, Usuda, Saku, Nagano	920	Qs, Cc
AC-61-1	A	2018.8.14	Mt. Tateshina-yama, Saku, Nagano	2054	Td
AC-63	A	2018.8.27	Mt. Tateshina-yama, Saku, Nagano	1992	Td
AC-43-1	A	2017.9.3	Lake side of Matsubara-ko, Koumi, Nagano	1206	Qs
AC-73	A	2018.8.29	Lake side of Matsubara-ko, Koumi, Nagano	1192	Qs
2100731-1	A	2010.7.31	Lake side of Komade-ike, Sakuho, Nagano	1320	Ah
S-125 (= TNS-F-61975)	A	2010.9.24	Lake side of Komade-ike, Sakuho, Nagano	1320	Ah
AC-64-1	B	2018.8.29	Lake side of Komade-ike, Sakuho, Nagano	1305	Qc, Bp
AC-64-2	B	2018.8.29	Lake side of Komade-ike, Sakuho, Nagano	1291	Bp
S-245 (= TNS-F-61977)	A	2011.8.4	Mugikusa-touge Pass, Koumi, Nagano	1930	Av, Td, Be
AC-68	A	2018.9.14	Azusayama, Kawakami, Nagano	1487	Qc, Fc
AC-48	B	2017.9.10	Enrei-kouen, Okaya, Nagano	1000	Qs
Okaya201108	B	2011.8.7	Osachi, Okaya, Nagano	870	Af
AC-23	B	2016.7.20	Mt. Eimeiji-yama, Chino, Nagano	1020	Qs, Pd
AY-220720-004	B	2020.7.20	Mt. Eimeiji-yama, Chino, Nagano	1015	Qs
S-46	A	2009.8.23	Mt. Amida-dake, Hara, Nagano	1850	Av, Qc
S-48 (= TNS-F-61972)	A	2009.8.23	Mt. Amida-dake, Hara, Nagano	1850	Av, Qc
AC-47-6	A	2017.9.8	Mt. Nishi-dake, Fujimi, Nagano	1751	Lk, Av, Bp, Qc
AC-34-1	B	2017.8.10	Ono, Tatsuno, Nagano	1009	Pd
AC-35-3	B	2017.8.10	Ono, Tatsuno, Nagano	1011	Pd
AC-54-8	B	2018.7.22	Ono, Tatsuno, Nagano	1011	Pd, Cc
Ahem080927 (= TNS-F-61970)	B	2008.9.27	Kayano-kougen, Minowa, Nagano	1200	Pd
AC-26-2	B	2017.7.26	Kayano-kougen, Minowa, Nagano	1178	Pd, Qs
AC-28-2	A	2017.7.28	Fujisawa, Takato, Ina, Nagano	1272	Pd, Qs
S-350	A	2013.9.21	Karei-kougen, Ina, Nagano	1850	Av
AC-8-1	A	2016.7.29	Karei-kougen, Ina, Nagano	1855	Av
AC-33	A	2017.8.10	Karei-kougen, Ina, Nagano	1853	Av
AC-5-1	B	2016.7.23	Chusenji, Ina, Nagano	989	Pd
AC-6-1	B	2016.7.24	Chusenji, Ina, Nagano	989	Pd, Qs
AC-30	B	2017.7.31	Chusenji, Ina, Nagano, Japan	989	Qs
AC-45	B	2017.9.5	Mt. Togura-yama, Komagane, Nagano	1503	Pd, Qc
AC-53	B	2018.7.14	Akaho, Komagane, Nagano, Japan	802	Pd, Qs
2070921Y	B	2007.9.21	Orikusa-touge Pass, Nakagawa, Nagano	1100	Qs
S-108 (= TNS-F-61974)	B	2009.7.19	Orikusa-touge Pass, Nakagawa, Nagano	1100	Pd, Qs
AC-21	B	2016.10.13	Orikusa-touge Pass, Nakagawa, Nagano	1159	Pd, Qs
AC-13	A	2016.8.25	Shirabiso-touge Pass, Iida, Nagano	1841	Av
AC-56	B	2018.7.26	Hyogoe-touge Pass, Iida Nagano	1154	Qs
Ahem080907 (= TNS-F-61969)	B	2008.9.7	Nezamenotoko, Agematsu, Nagano	700	Qs, Pd, Af
AC-18-2	A	2016.10.2	Hiwada-kougen, Takayama, Gifu	1375	Qc, Bp
S-248 (= TNS-F-61978)	A	2011.8.12	Mt. Amigasa-yama, Hokuto, Yamanashi	1550	Ah
AC-31	A	2017.8.2	Mt. Amigasa-yama, Hokuto, Yamanashi	1570	Pd
AC-46	A	2017.9.8	Mt. Tennyo-yama, Hokuto, Yamanashi	1321	Qc
AC-55	B	2018.7.25	Mt. Kayaga-take, Kai, Yamanashi	1019	Qs
S-321	A	2012.10.6	Mt. Nagao-yama, Narusawa, Yamanashi	1380	Pd, Lk, Ah
S-323 (= TNS-F-61982)	A	2012.10.6	Mt. Fuji-san, Narusawa, Yamanashi	1600	Av
AC-38-1	A	2017.8.22	Mt. Fuji-san, Fujiyoshida, Yamanashi	1543	Av
AC-38-3	A	2017.8.22	Mt. Fuji-san, Fujiyoshida, Yamanashi	1609	Av
AC-39-4	B	2017.8.22	Fujiyoshida, Yamanashi	934	Pd
S-325	B	2012.10.6	Hachioji, Tokyo	288	Qg
S-327 (= TNS-F-61983)	B	2012.10.6	Hachioji, Tokyo	288	Qs
AY-2140716	B	2014.7.16	Hachijo-jima Island, Tokyo	302	Cs
Hongo 5297 (= OSA-MY100271)	B	1975.7.30	Nango-imodani, Ohtsu, Shiga	150	Qa, Qs
AC-17	B	2016.9.22	Tsuegayabu, Kouya, Wakayama	505	Q
AC-14-1	B	2016.9.16	Mt. Konrai-san, Iwade, Wakayama	200	Q
AC-22	B	2016.7.16	Tottori, Tottori	66.5	Cs
S-77	B	2010.7.7	Mt. Oo-dake, Nakatsu, Oita	350	Cs
S-78	B	2010.7.7	Mt. Takabase-yama, Yufu, Oita	150	ND
AC-71	B	2018.9.15	Shonai, Yufu, Oita	435	Qs
S-70 (= TNS-F-61973)	B	2010.6.27	Mt. Karakuni-dake, Kobayashi, Miyazaki	1451	ND
MarN20170515-01	B	2017.5.12	Mt. Yonaha-dake, Kunigami, Okinawa	333	Cs
SCF20140912-251	A	2014.9.12	Inje County, Gangwon Province, South Korea	ND	ND
LE203026 (Lectotype)	A	1945.8.23	Near Primorskaya, Ussuriysk, Russia	ND	Q
Amanita caesarea					
BL-1		2012.1	Bulgaria (commodity)	ND	ND
SP-1		2007.12	Spain (commodity)	ND	ND
Amanita kitamagotake					
S-76 (= TNS-F70006)		2009.7.16	Aoba-kouen, Oita, Oita	95	ND
S-329 (= TNS-F70011)		2012.10.8	Hachioji, Tokyo	288	Qs
Amanita chatamagotake					
EN-66		2009.7.16	Aoba-kouen, Oita, Oita	95	ND
S-222 (= TNS-F70016)		2011.7.12	Aoba-kouen, Oita, Oita	95	ND
Amanita rubromarginata					
S-207		2011.6.3	Banna-kouen, Ishigaki-jima Island, Okinawa	70	ND
Amanita esculanta					
EN-28		2009.6.14	Ohshiba-kouen, Minami-minowa, Nagano	800	Pd

[a] The indicated "A" and "B" following each specimen mean phylogenetic groups explanted in the result section.
[b] Specimens sampled outside Japan was indicated the country.
[c] Af: *Abies firma*, Ah: *Abies homolepis*, Am: *A. mariesii*, As: *A. sachalinensis*, Av: *A. veitchii*, Be: *Betula ermanii*, Bp: *B. platyphylla* var. *japonica*, Cc: *Castanea crenata*, Cs: *Castanopsis sieboldii* subsp. *sieboldii*, Fc: *Fagus crenata*, Lk: *Larix kaempferi*, Pa: *Picea abies*, Pd: *Pinus densiflora*; Pp: *P. parviflora* var. *pentaphylla*, Qa: *Quercus acutissima*, Qc: *Q. crispula* var. *crispula*, Qg: Q. glauca, Qs: *Q. serrata*, Q: *Quercus* sp., Td: *Tsuga diversifolia*, ND: not determined.

Table 3. Primers used for the PCR for the targeted 6 loci.

Targeted locus	Primer name	Sequence (5'→3')	References
nuc rDNA ITS	ITS1-F (f)		1
	LB-W (r)		2
nuc rDNA IGS1	CNL12 (f)		3
	5s-Anderson (r)		4
	IGS1-AcoidesF	GAGCTTTGGGATGTGTTGTGGAGA	10
	IGS1-AcoidesR	CTTGGGTTCAGGCAGAGTCAGAGG	10
β-TUB	*β-tub*-AcoidesF	AAGTGGAGCRGGGAACAAYTGG	10
	β-tub-AcoidesR	CRAGYTGGTGAACMGAGAGWG	10
	β-tub-Acoides2F	CTAGAGCCTGGTACCATGGA	10
	β-tub-Acoides2R	GCAGATGTCGTACAGAGCTT	10
RPB2	bRPB2-6F (f)		5
	bRPB2-7.1R (r)		5
	rpb2-AcoidesF	CGTCAACGGAGTATGGATG	10
	rpb2-AcoidesR	TCTGAACTCTTCGCCTTCGT	10
TEF1	tef-1F (f)		6
	tef1-R (r)		6
	tef-2218R(r)		7
	tef-983F (f)		7
	tef1-AcoidesF	CATCTCAAGCTGATTGTGCCAT	10
	tef1-Acoides2R	TCAATGGCATCAAGAAGG	10
	tef1-UF	AGCTGGTATCTCCAAGGACGG	10
	tef1-AcoidesR	GAAKCGATCTTCGRTCCACT	10
COX3	COX3-1		8
	COX3-2		8
	cox3-AcoidesF	GCTGGAAATAGAAAAGCTGCAA	10
	cox3-AcoidesR	TAAGCCGTGAAGACCCGTAG	10
ATP6	ATP6-AmF	GGTTTAAATGCTCCTATTTTAGGTC	9
	ATP6-AmR	GRAAATAATCTAACTCCTAATGA	9

1: Gardes & Bruns (1993); 2: Tedersoo et al. (2008); 3: Anderson & Stasovski (1992); 4: Duchesne & Anderson (1990); 5: Matheny (2005); 6: Morehouse et al. (2003); 7: Rehner & Buckley (2005); 8. Kretzer & Bruns (1999); 9: This study (The sequences were designated from genome data of *Amanita muscaria* (L.) Lam (*A. muscaria* Koide BX008) reported by Kohler et al., 2015.); 10: This study.

Acoides2R primers with an initial denaturation step at 95 °C for 3 min followed by 40 cycles of denaturation at 95 °C for 30 s, annealing at 50 °C for 30 s, and extension at 72 °C for 1 min, with a final extension step at 72 °C for 7 min. To amplify *RPB2* from the Hongo 5297 specimen, PCR was conducted with an initial denaturation step at 95 °C for 3 min followed by 40 cycles of denaturation at 95 °C for 30 s, annealing at 60 °C–54 °C (cycles 1–5 at 60 °C, 6–10 at 58 °C, 11–20 at 56 °C, and 21–35 at 54 °C) for 30 s, and extension at 72 °C for 1 min, with a final extension step at 72 °C for 7 min. Second-round PCR was conducted using the following primer pairs and annealing temperatures: IGS1, IGS1-AcoidesF/IGS1-AcoidesR (57 °C); *β-TUB*, *β-tub*-AcoidesF/*β-tub*-AcoidesR (53 °C) or *β-tub*-Acoides2F/*β-tub*-Acoides2R (55 °C); *RPB2*, *rpb2*-AcoidesF/*rpb2*-AcoidesR or *rpb2*-AcoidesF/*rpb2*-AcoidesR′ (both 51 °C); *TEF1*, *tef1*-UF/*tef1*-AcoidesR′ (53 °C); and *COX3*, *cox3*-AcoidesF/*cox3*-AcoidesR (50 °C). PCR amplicons were subjected to electrophoresis on 1.5–2.0% agarose gels to confirm amplification specificity, and then purified using a QIAquick PCR Purification Kit (Qiagen, Hilden, Germany). If necessary, bands for targeted amplicons were excised from the gel and extracted using a QIAquick Gel Extraction Kit (Qiagen) for further DNA analyses.

A BigDye Terminator v. 3.1 Cycle Sequence Kit (Thermo Fisher Scientific) with primers identical to the sequences used for first- or second-round PCR was used for cycle sequencing with a ProFlex 3 × 32-well PCR System (Applied Biosystems). The amplicons were purified by ethanol precipitation and sequenced directly using an ABI 3130 Genetic Analyzer (Applied Biosystems). The sequences were edited using SeqScanner software v. 2.0, and then assembled using CLUSTALW (http://www.genome.jp/tools-bin/clustalw). We confirmed nucleotide complementarity between the two strands and registered the sequences in the DNA Data Bank of Japan (DDBJ; https://www.ddbj.nig.ac.jp/index.html). As the IGS1 region of *A. caesareoides* was not directly sequenced, DNA cloning was performed using a Mighty TA-cloning Kit (TaKaRa) in accordance with the manufacturer's recommendations.

2.5. Phylogenetic analyses

The reddish-pileus *A. caesareoides*, *A. caesarea*, and *A. jacksonii* Pomerl. were subjected to phylogenetic analyses. In addition, sequences of related species in section *Caesareae* were included in the phylogenetic analyses (Supplementary Table S2). The following data sets were constructed for each of the seven loci: *A. caesareoides*, *A. jacksonii*, *A. caesarea*, *A. basii* Guzmán & Ram.-Guill., *A. A. kitamagotake*, *A. fuscoflava* Zhu L. Yang, Y.Y. Cui & Q. Cai, *A. subhemibapha* Zhu L. Yang, Y.Y. Cui & Q. Cai, and *A. rubroflava* Y.Y. Cui, Q. Cai & Zhu L. Yang for ITS; *A. caesareoides*, *A. jacksonii*, *A. caesarea*, and *A. chatamagotake* for IGS1; *A. caesarea*, *A. caesareoides*, and *A. jacksonii* for *β-TUB*; *A. caesareoides*, *A. jacksonii*, *A. caesarea*, *A. kitamagotake*, *A. vernicoccora* Bojantchev & R.M. Davis, *A. rubroflava*, *A. subhemibapha*, and *A. chatamagotake* for *RPB2*; *A. caesarea*, *A. caesareoides*, *A. jacksonii*, *A. chatamagotake*, *A. basii*, *A. rubroflava*, and *A. rubromarginata* Har. Takah. for *TEF1*; *A. caesareoides*, *A. jacksonii*, *A. caesarea*, *A. kitamagotake*, and *A. chatamagotake* for *ATP6*; and *A. caesareoides*, *A. jacksonii*, *A. caesarea*, *A. kitamagotake*, *A. chatamagotake*, and *A. esculenta* Hongo & I. Matsuda for *COX3*. DNA sequences were aligned using MUSCLE (Edgar, 2004) in MEGA v. 7.0 (Kumar et al., 2016) and manually edited. Phylogenetic trees were constructed based on the maximum-likelihood (ML) analysis using W-IQ-TREE (Trifinopoulos et al., 2016). For the ML analysis, the F81+F+I model for ITS1, the JC model for 5.8S and ITS2, the K2P+I model for IGS1,

the L2P model for *β-TUB*, the K2P+I model for *RPB2*, the TIM2e+G4 model for *TEF1*, the F81+F+I model for *ATP6* and *COX3* were selected by ModelFinder (Kalyaanamoorthy et al., 2017) as the substitution models for each single data set.

To construct a concatenated phylogenetic tree based on data from six DNA loci, we set a partition scheme for an alignment comprised of all loci using PartitionFinder2 v. 1.1. (Lanfear et al., 2017). Under the "greedy" search algorithm in PartitionFinder2 (Lanfear et al., 2012), we estimated the optimal partition consisting of 10 subsets (Supplementary Table S3). This partition scheme was well supported by biological information (e.g., genomic or mitochondrial DNA, or coding or intronic region) of the loci examined. ModelFinder assigned an independent substitution model for each subset, and substitution rates were calculated independently in phylogenetic analysis complemented by W-IQ-TREE. Branch support was evaluated by bootstrap analysis with 1000 replicates using the ultrafast bootstrap option (UFboot; Minh et al., 2013), approximate Bayesian test (aBayes; Anisimova et al., 2011), and SH-aLRT branch test (Guindon et al., 2010). We set *A. chatamagotake* as the outgroup taxon for each data set, except for the nuc rDNA ITS tree, in which *A. chatamagotake* showed far too high divergence compared to *A. caesareoides* and its relatives. Phylogenetic trees were edited in FigTree v. 1.4.4 (http://tree.bio.ed.ac.uk/software/figtree/).

2.6. Divergence time estimation

The alignments of nuc rDNA ITS and IGS1, *β-TUB*, *RPB2*, *TEF1*, *ATP6*, and *COX3* for the two phylogenetic clades of *A. caesareoides*, as well as the North American *A. jacksonii* and the Mediterranean *A. caesarea*, were used for divergence time estimation. Bayesian estimation of species divergence time was performed using BEAST v. 2.6.2 (Drummond & Bouckaert, 2015). All alignment files were separately imported into BEAUti. The gene partitions were set to be unlinked for substitution models and linked for molecular-clock models and gene trees. The coalescent constant population model was implemented under gamma distributed prior (shape = 1.0, scale = 0.001, offset = 0). The clock model was applied as a relaxed clock log normal model, and the prior value of clock rate was set to 3.93×10^{-3}/Mya, which was estimated from the highest gap of substitution rates among the four clades (ca 1.0×10^{-3}/Mya) as well as the calculation from primary analysis by BEAST. According to the substitution models for BEAST, the substitution rates, shape parameter of the gamma distribution, and proportion of invariant sites (for "I") were estimated by Bayesian inference analysis using MrBayes v. 3.2.7 (Ronquist et al., 2012). We assigned the optimal substitution model for each of 10 schemes implemented in PartitionFinder2 (Supplementary Table S3). For fossil node calibrations, we used gamma-distributed priors (shape = 1.0, scale = 1.0, offset = 6.0 for stem node) following the molecular dating in Sanchèz-Ramiréz et al. (2015a), in which *A. jacksonii* and the Japanese *A. hemibapha* lineages branched from their ancestral lineage approximately 7–9 Mya. The posterior distributions of parameters were obtained by Markov chain Monte Carlo analysis for 10 million generations with a burn-in percentage of 10%. The Markov chain Monte Carlo result was confirmed using Tracer v. 1.6. The relationships among samples from the posterior distributions were summarized as a maximum clade credibility tree with the maximum sum of posterior probabilities listed on the internal nodes using TreeAnnotator v. 2.6.2 (Drummond & Bouckaert, 2015); the posterior probability limit was set to 0.5 to summarize the mean node heights. FigTree v. 1.4.4 was used to visualize the constructed tree, and mean divergence times were calculated using 95% highest posterior density intervals. For expected geological age, we referred to the international chronostratigraphic chart (Cohen et al., 2013).

3. Results

3.1. Phylogenetic position of Tamagotake specimens

The aligned data sets of ITS, IGS1, *β-TUB*, *RPB2*, *TEF1*, *ATP6*, and *COX3* consisted of 644, 1204, 378, 706, 489, 795, and 735 bp, respectively. After the exclusion of ambiguous aligned sites from the phylogenetic analyses, these data sets consisted of 538, 849, 378, 457, 475, 408, and 497 bp, respectively (TreeBASE accession no. S29648). The sequences of the lectotype LE203026 and Hongo 5297 were not used in phylogenetic analyses in most cases because of their limited length (Table 4).

According to the ITS phylogenetic tree (Fig. 2), all tested specimens of *A. caesareoides* formed a single clade with its lectotype, which was distinct from closely related *A. caesarea* and *A. jacksonii*, consistent with the results of Endo et al. (2016). In the phylogenetic trees of *β-TUB* (Supplementary Fig. S1), *RPB2* (Fig. 3), *TEF1* (Fig. 4), *ATP6* (Supplementary Fig. S2), *A. caesareoides* specimens were separated into two groups (phylogroups A and B), which were supported by the statistical tests (SH-aLRT, aBayes, and UFboot). The *COX3* phylogenetic tree (Supplementary Fig. S3) also encompassed *A. caesareoides* phylogroups A and B, and the former was strongly supported as a clade by the aBayes and UFboot tests. Similarly, the IGS1 phylogenetic tree (Supplementary Fig. S4) demonstrated the separation of *A. caesareoides* into phylogroups A and B, although the latter had three subclades supported by two or single statistical tests. Although the *β-TUB*, *TEF1*, and *RPB2* phylogenies suggested distinct positions for phylogroups A and B of *A. caesareoides* in relation to *A. caesarea* and *A. jacksonii*, respectively, the *ATP6* and *COX3* trees displayed a continuum between phylogroup A and *A. caesarea* (Supplementary Figs. S2, S3) and a continuum between phylogroup B and *A. jacksonii* (Supplementary Fig. S3), respectively. No probable hybrid specimen between phylogroups A and B was observed in *A. caesareoides*. The concatenated phylogenetic tree, which was comprised of six DNA loci, showed that *A. caesareoides* could be divided into phylogroups A and B, with statistically significant values as a clade (Fig. 5). In this tree, *A. jacksonii* first branched from the clade including three others; second, *A. caesareoides* phylogroup B branched from the clade including the other two; and third, branched into *A. caesareoides* phylogroup A and *A. caesarea* (Fig. 5).

Although the lectotype LE203026 of *A. caesareoides* yielded only partial sequences of IGS1, *RPB2*, and *COX3* (and no sequences of *β-TUB*, *TEF1*, and *ATP6*), these sequences showed greater identities to the sequences of phylogroup A (99.3–100%) than to the sequences of phylogroup B (94.7–99.6%) (Table 4). The *A. caesareoides* Hongo 5297 specimen yielded only a partial sequence of *TEF1*, which showed higher homology to phylogroup B (100%) than to phylogroup A (97.0%) (Table 4). Therefore, *A. caesareoides* phylogroup A was regarded as true *A. caesareoides*. In contrast, *A. caesareoides* phylogroup B was presumed to correspond to *A. hemibapha* sensu Hongo (Hongo, 1975, 1982).

Two distinct phylogroups of *A. caesareoides* showed different host associations (Figs. 3, 4; Supplementary Figs. S1–S4; Table 2; Supplementary Table S2). Specimens in phylogroup A generally showed associations with subalpine and cool-temperate *Pinaceae*, *Betulaceae*, and *Fagaceae* (deciduous species) as canopy trees. In contrast, specimens in phylogroup B typically showed associations with temperate-to-subtropical *Pinaceae*, *Betulaceae*, and *Fagaceae* (deciduous and evergreen species) as canopy trees.

Table 4. Comparison of sequences of several DNA loci in the lectotype LE203026 of *Amanita caesareoides* (Vassiljeva, 1950) and a specimen Hongo 5297A of *A. hemibapha* (Hongo, 1975).

DNA loci	Phylogroup	Representative specimens of *A. caesareoides*	Homology of sequence (%) of the compared specimens*		Aligned sequence	
			LE203026	Hongo 5297	Length (bps)	Position**
RPB2	A	AY-2150918-011	100	ND	244	201–444
		S-125	99.6			
		S-46	99.6			
	B	AC-36	94.7	ND	244	201–444
		Ahem080907	96.3			
		S-327	96.3			
COX3	A	AY-2150918-011	99.3	ND	144	450–593
		S-125	100			
		S-46	100			
	B	AC-36		ND	144	450–593
		Ahem080907	97.9			
		S-327				
IGS1	A	AY-2150918-011		ND	281	379–659
		S-125	100			
		S-46				
	B	AC-36_clone6	99.3	ND	281	379–659
		AC-36_clone7	99.3			
		AC-36_clone9	99.6			
		Ahem080907	99.6			
		S-327_clone1	99.3			
		S-327_clone2	98.6			
		S-327_clone3	98.9			
TEF-1	A	AY-2150918-011		97.0	101	34–134
		S-125	ND			
		S-46				
	B	AC-36		100	101	34–134
		Ahem080907	ND			
		S-327				

*ND: No sequence was obtained due to almost no amplification by PCR.
**Base number from the initial of forward primer: bRPB2-6F for *RPB2*, COX3-1 for *COX3*, CNL12 for IGS1, TEF1/tef-983F for *TEF-1*, respectively.

3.2. Estimation of the evolutionary pattern of the two phylogroups of A. caesareoides

We estimated the evolutionary time scale of the speciation of two *A. caesareoides* phylogroups, based on the evolutionary pattern among species in the section *Caesareae* reported by Sánchez-Ramírez et al. (2015a). The seven-locus phylogenetic tree showed that the ancestral lineage of *A. caesareoides* and *A. caesarea* branched from the *A. jacksonii* lineage at 6.00–8.48 Mya in 90% highest posterior density (prior value; Fig. 6), which branched into two (lineages I and II) at around 2.38–7.54 Mya, one of which (lineage I) further branched into two (i.e., *A. caesareoides* phylogroup A and *A. caesarea*) at 0.88–4.02 Mya.

3.3. Geographic distributions and habitats of the two A. caesareoides phylogroups

The distributions of *A. caesareoides* phylogroups A and B differed. Phylogroup A was sampled from subalpine to cool-temperate areas of Hokkaido and higher elevation areas of Honshu Island (840–2052 m above sea level), whereas phylogroup B was sampled from cool-temperate to subtropical areas of Hokkaido, Honshu, Kyushu, and Okinawa islands. Therefore, we regarded phylogroup A as a high-elevation (HE) population, and phylogroup B as a low-elevation (LE) population. To assess how WI, CI, and MAT explain the different geographic distributions of the HE and LE populations, regression lines were generated between altitude and the temperature indices in samples from Hokkaido, Honshu, and Kyushu islands (Fig. 7; Supplementary Fig. S5). The regression coefficient (R) tended to be higher in WI (Fig. 7). The slopes of regression lines slightly differed according to topography: the HE population in Honshu was distributed in mountainous areas and showed a steep slope of the regression line, whereas the LE populations in Honshu and Kyushu were distributed in both mountainous and plains areas and showed a gentle slope of the regression line. Furthermore, the HE population in Hokkaido was distributed in both mountainous and plains areas, and the slope of its regression line was similar to that of the LE population. The habitats of the HE and LE populations had WI values of 37.0–71.0 and 57.3–188.2, respectively (Fig. 7; Supplementary Table S1). Therefore, the HE and LE populations had overlapping distributions in central Honshu (WI 57.3–71.0; within the cool-temperate range). No sample of an HE population was collected in a warm-temperate area, and no sample of a LE population was collected in a subalpine area. The LE population was abundant at lower elevations in Honshu, dominant in the southern area, and was observed at only one site in Hokkaido, Sapporo, Atsubetsu. No sample of an HE population was collected in western Japan.

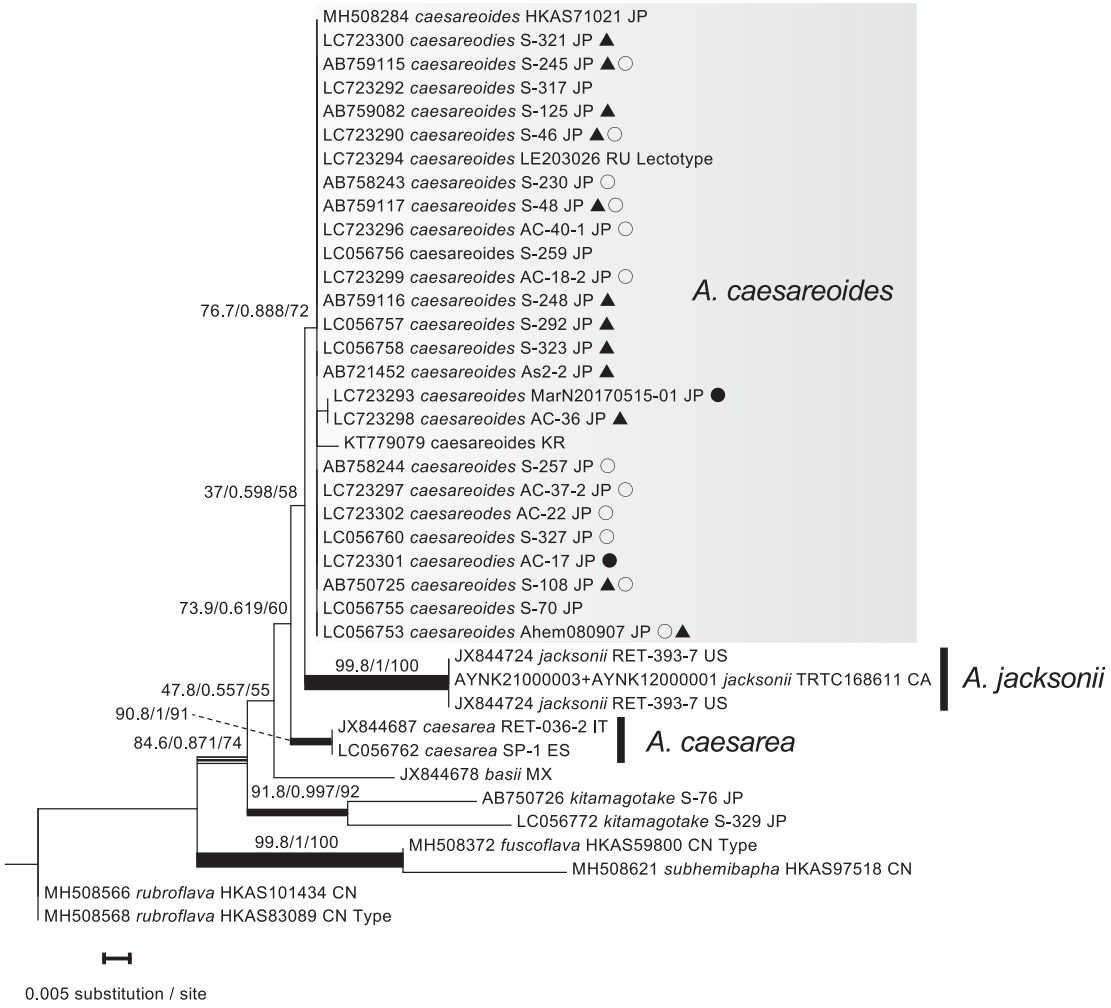

Fig. 2 – Maximum likelihood (ML) phylogenetic tree of *Amanita* section *Caesareae* based on nuc rDNA ITS sequences using the F81+F+I and JC substitution models. Values at each node are percentages of SH-aLRT branch test (SH-aLRT), approximate Bayesian posterior probability (aBayes), and ultrafastbootstrap support (UFBoot). Thick-line nodes indicate fully significantly supported branches: SH-aLRT ≥ 80%, aBayes ≥ 0.95, and UFBoot ≥ 95%. Secondary thick-line nodes and the set of three thin-line nodes indicate branches supported by two or one of three statistical tests, respectively. Notations following accession numbers and species epithets are specimen IDs, localities, and putative host-tree taxa. JP, Japan; SK, South Korea; RU, Russia; US, United States of America; CA, Canada; MX, Mexico; IT, Italy; ES, Spain; BG, Bulgaria. Closed circle, ever-green *Fagaceae* tree; open circle, deciduous *Fagaceae* tree; closed triangle, *Pinaceae* tree; Abi, *Abies*; Lar, *Larix*; Pic, *Picea*; Pin, *Pinus*; Bet, *Betula*; Cae, *Castanea*; Cao, *Castanopsis*; Fag, *Fagus*; Que, *Quercus*.

3.4. Sympatric distribution of the two A. caesareoides populations in a mountain area

To assess the importance of the probable absence of a hybrid between HE and LE populations of *A. caesareoides*, as well as the distinct vertical patterns within each local region, we compared the two populations in the Myoko Volcano Group (Hayatsu et al., 1994), Yatsugatake Mountains and the marginal ranges, and Ina Mountains and the marginal ranges of the Akaishi Mountains (Figs. 8, 9). The sympatric distributions of the two populations in these three areas were expected to be within the WI values of 67.9–71.5, 61.5–68.4, and 57.3–67.9, respectively. In the Myoko Volcano Group, the slopes of the regression lines differed slightly between the two populations (Fig. 9A–C). Therefore, in higher elevation areas within the overlapping distribution, the LE population was expected to be distributed at higher WI sites, whereas the HE population was expected to be distributed at lower WI sites. However, in the other two regions, the slopes of regression lines did not exhibit large differences (Fig. 9D–I), suggesting that the HE and LE populations were equally present in the sympatric areas. In fact, four forest sampling sites (i.e., Mt. Madarao-san and the lakesides of Reisenji-ko, Matsubara-ko, and Komade-ike) harbored both populations sympatrically. At these sites, the overlapping WI ranges were 65–66, 65–66, 67–68, and 59–60, respectively.

3.5. Physiological characteristics of the two A. caesareoides phylogroups

Samples of *A. caesareoides* HE population showed mycelial growth on MNC agar, and their mycelia were subcultured on MNC agar. However, samples of LE population showed limited mycelial growth, typically only on the surface of the mycelial inoculum (basidioma tissue). Therefore, mycelium of the LE population could not be subcultured on MNC agar. The mycelial growth rate from the mycelial inoculum onto MNC agar was significantly different between the populations ($P < 0.05$; Table 5; Supplementary Table S4).

Mycelial colonies of an *A. caesareoides* HE population on MNC agar were white to light yellow, irregular in shape, and had a filamentous margin (Fig. 10A–C). Generative hyphae of the colony

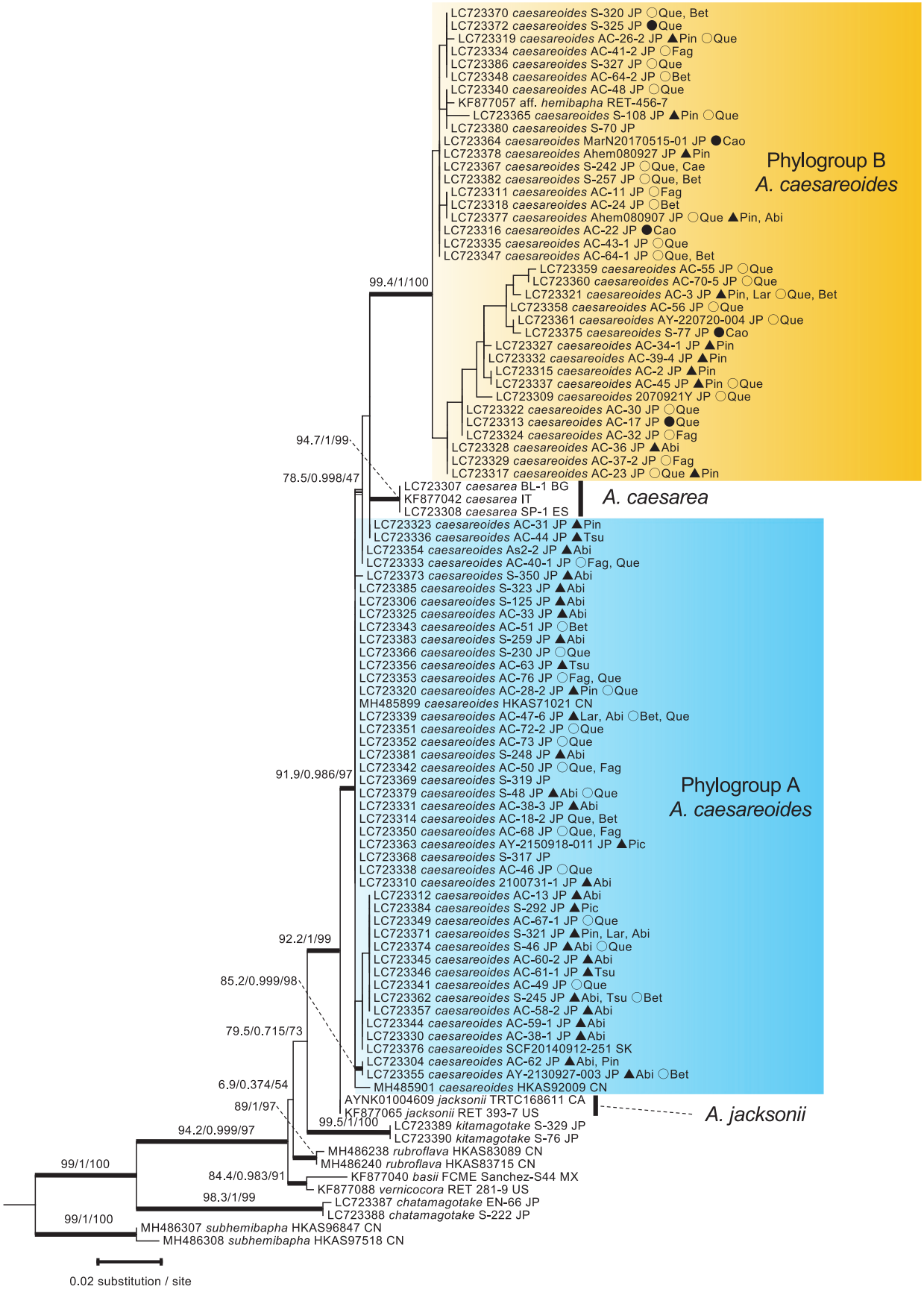

Fig. 3 – Maximum likelihood (ML) phylogenetic tree of *Amanita* section *Caesareae* based on *RPB2* sequences using the K2P+I substitution model. The tree was constructed based on the data of exon regions. Other notations are as in Fig. 2.

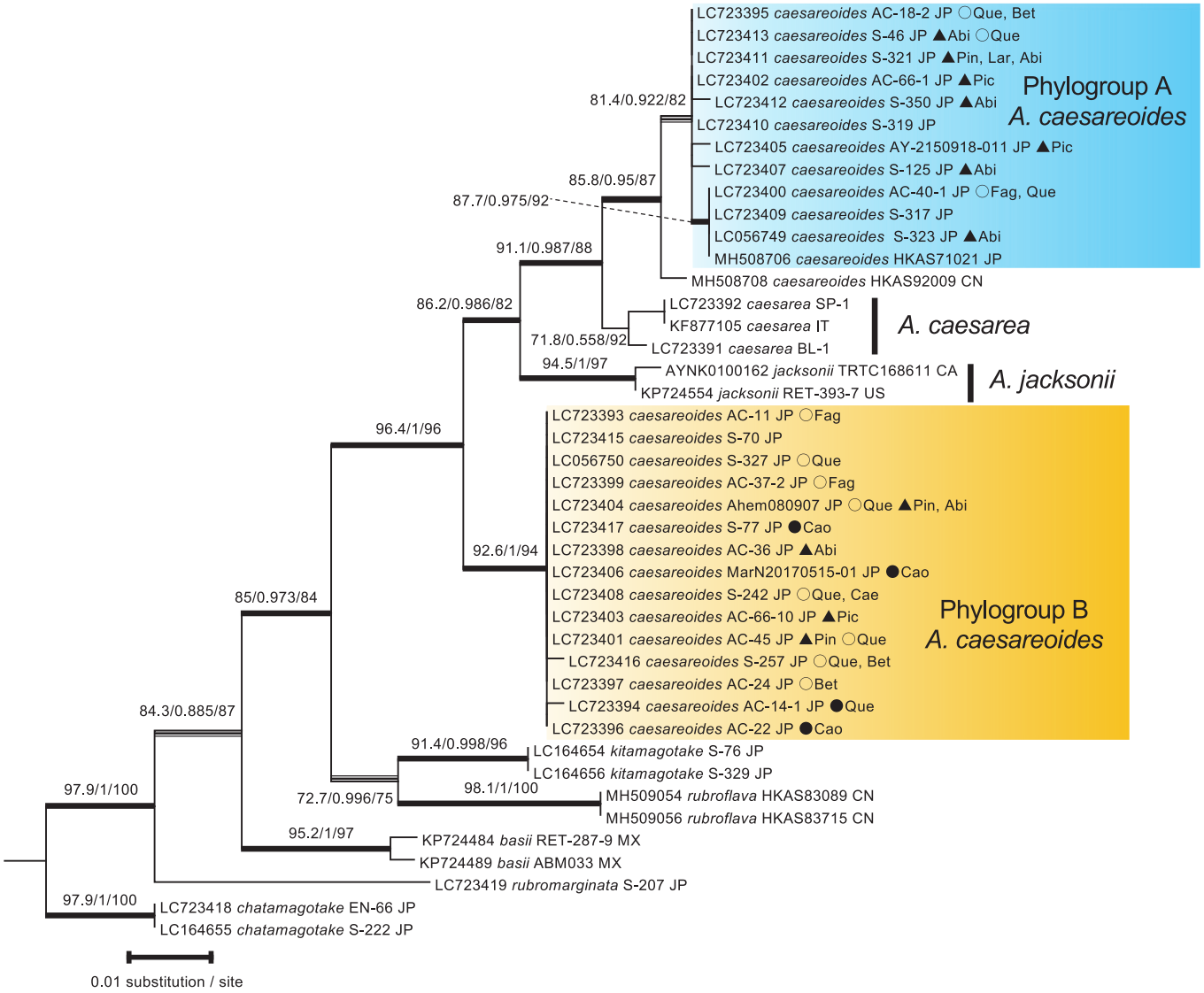

Fig. 4 – Maximum likelihood (ML) phylogenetic tree of *Amanita* section *Caesareae* based on *TEF1* sequences using the TIM2e+G4 substitution model. The tree was constructed based on data on both intron and exon regions. Other notations are as in Fig. 2.

margin were straight or interwoven, 1.6–5.6 μm in diam, sometimes inflated intercalary or terminally with a chlamydospore or monilioid cell-like structure (Fig. 10G, H). Although knobs of hyphae were sometimes present, no clamp connections were observed. Mycelial colonies of an *A. caesareoides* LE population on MNC agar were white to ochre-yellow in color, irregular in shape, and had a flat and undulate margin (Fig. 10D–F). Generative hyphae of the colony margin were straight and 1.7–5.7 μm in diam. In addition, chlamydospore or monilioid cell-like swellings were observed at the termini of generative hyphae, which were 8.6–46.3 μm in length and 7.5–31.7 μm in width (Fig. 10I, J). Some terminal swellings burst (Fig. 10I). No clamp connections were observed.

3.6. Morphology of basidiomata of the two populations labeled with the name A. caesareoides

The lengths of 50 spores, 30 basidia, 10 sterigmata, and 10 cells on the lamella margin of 26 specimens of *A. caesareoides* HE population (including the lectotype), 29 specimens of LE population (including Hongo 5297—used in the taxonomic study to describe Japanese *A. caesareoides* [Hongo, 1975]) were measured (Supplementary Table S5). Based on the species delimitation criterion for the section *Caesareae* (Endo et al., 2016, 2017; Yang, 2005), the two *A. caesareoides* populations did not show substantial morphological differences. However, the mean spore size was significantly larger in the HE population ($P < 0.01$; Table 5) and the mean sterigmata length tended to be greater in the HE population ($P = 0.0579$; Table 5).

Based on the phylogenetic positions and the ecological, physiological, and morphological differences of the two populations of "*A. caesareoides*", we regarded them as two distinct species. As the *A. caesareoides* HE population included the *A. caesareoides* lectotype, we describe the LE population as a new *Amanita* species.

4. Taxonomy

Amanita satotamagotake M. Kodaira, N. Endo & A. Yamada, sp. nov.

Fig. 11

MycoBank no.: MB 845966.

Diagnosis: This species is cryptic against *A. caesareoides* but can be distinguished by the *β-TUB*, *RPB2*, *TEF1*, *ATP6*, *COX3*, and IGS1

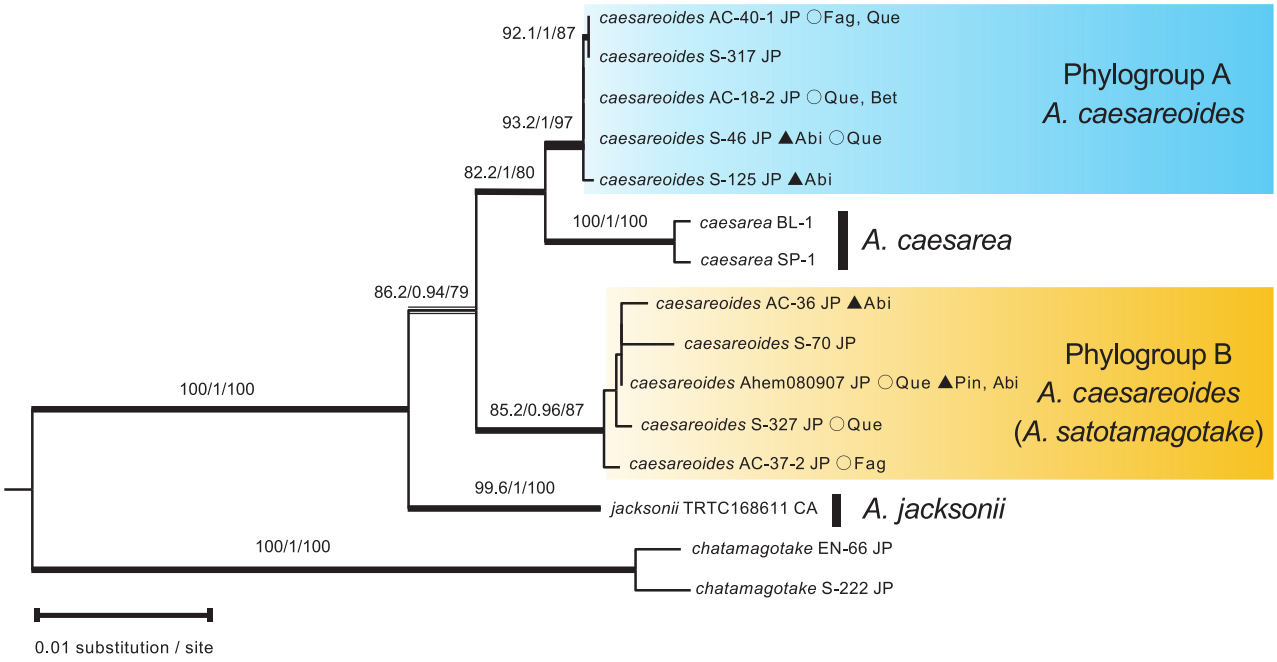

Fig. 5 – Maximum likelihood (ML) phylogenetic tree of *Amanita* section *Caesareae* based on concatenate sequences of six DNA loci. Details of the calculation are provided in Supplementary Table S3. Other notations are as in Fig. 2.

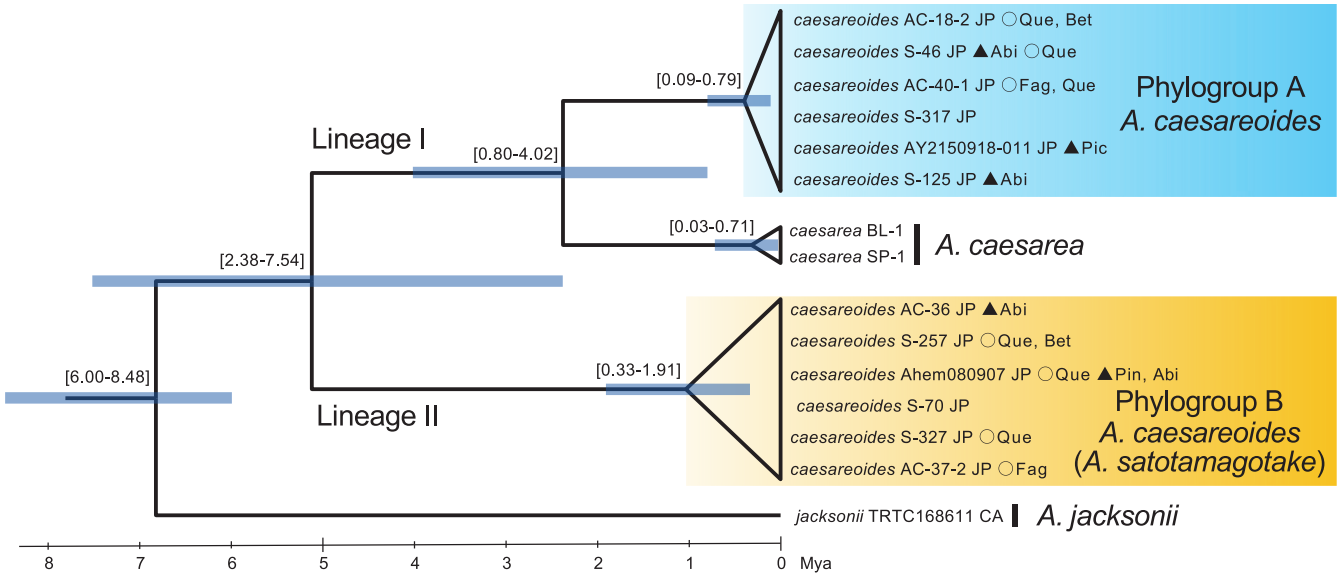

Fig. 6 – Chronogram and estimated divergence times of *Amanita* section *Caesareae* by molecular clock analysis of seven DNA loci. The chronogram calibration point is based on the divergence times of *A. jacksonii* and the *A. caesareoides–A. satotamagotake–A. caesarea* lineage at 6.00–8.48 Mya. Blue bars, 95% confidence interval. Other notations are as in Fig. 2.

of nuc rDNA phylogenies.

Type: JAPAN, Miyagi Pref., Shichigahama, Hanabushi-shrine, on the ground in a forest of *Abies firma*, 14 Oct 2017, coll. N. Endo (holotype, specimen ID: AC-36; TNS-F-82293).

Gene sequences ex-holotype: **LC723298** (ITS), **LC723439**–**LC723441** (IGS1), **LC779172** (*β-TUB*), **LC723328** (*RPB2*), **LC723398** (*TEF1*), **LC723507** (*ATP6*), **LC723491** (*COX3*).

Etymology: *satotamagotake* is the set of "sato" and "tamagotake," the former means "secondary forests and the surrounding village areas at the foot of mountains" in Japanese.

Description: ***Pileus*** 34–107 mm in diam, ovate when young or convex, then convex-umbonate to plano-convex-umbonate; surface red or reddish orange, sometimes orange, smooth, glabrous, viscid when moist; margin striation 12–26 mm in length, diam ratio 0.15–0.28(–0.38), sulcate–striate; color gradient between center to margin absent or slightly darker in center. ***Lamellae*** 6–10 mm in width at the center, dense; surface pale yellow, edge yellow, pale yellow, or orange. ***Stipe*** 106–232 mm in length, upper portion 6–13 mm in width, basal portion 10–14(–17) (–18) mm in width, cylindrical or tapering upward, stuffed when young, then hollow; surface pale yellow, yellow or cream, mostly covered with orangish or pale orangish, fiber-like patches toward the base, sometimes lacking in the patch. ***Annulus*** membranous, upper surface sulcate–striate, concolorous or slightly deeper than the stipe, lower surface smooth, slightly lighter than upper. ***Volva*** 32–59(–81) mm in height, 12–31 mm in width, saccate, ellipsoid, elongate or cylindrical, membranous; outer surface whitish; inner surface whitish or pale yellow. ***Basidiospores*** [1000 spores/10 basidiomata/9 speci-

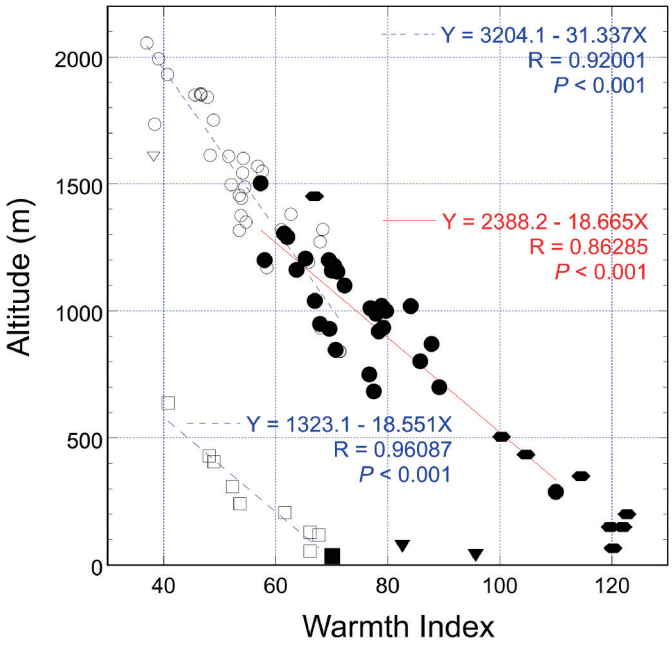

Fig. 7 – Distribution pattern of two *Amanita caesareoides* populations as indicated by warmth index (WI) and altitude. Open and closed symbols, sampling sites of HE and LE populations, respectively. Square, Hokkaido Island; triangle Tohoku Region of Honshu Island; circle, central and western Honshu Island; trapezoid, Kyushu Island. Samples from Izu Islands (WI 154.9) and Ryukyu Islands (WI 188.2) are not plotted. Regression lines are shown for HE populations (dotted blue lines) from Hokkaido and central Honshu Island, and for an LE population (red line) from central and western Honshu Island.

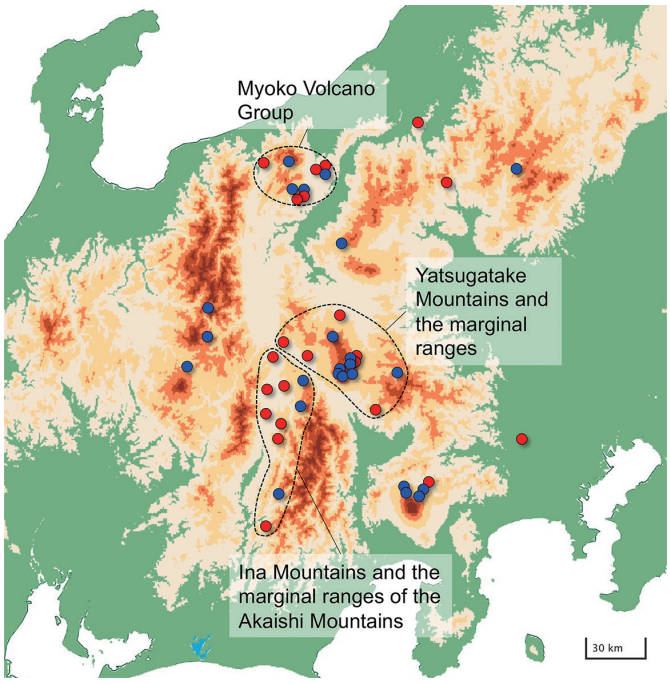

Fig. 8 – Distribution of two *Amanita caesareoides* populations (HE and LE) in the central region of Honshu Island. Blue and red circles indicate sampling sites of HE and LE populations, respectively. Sampling regions in the Myoko Volcano Group, Yatsugatake Mountains and marginal ranges, and the Ina Mountains and marginal ranges of the Akaishi Mountains are indicated by dotted lines. See Fig. 1 for map details.

mens] 6.9–10.9 × 5.5–8.8 [$L_m \times W_m$ = 7.9–8.6 × 6.6–7.2], Q = 1.03–1.46, Q_m = 1.18–1.23, subglobose, broadly ellipsoid, thin-walled, with one or several oily droplets, hyaline, non-amyloid; apiculus cubic. ***Basidia*** [270/9/8] 32.2–67.7 µm × 6.4–13.8(–15.0) µm [$L_m \times W_m$ = 38.5–48.2 × 8.2–10.9(–12.0)], cylindrical or clavate, 4-spored, rarely 1- or 2-spored, thin-walled, containing some oily droplets, hyaline, clamp connection present at the basal septum; sterigma 1.3–6.5×1.0–2.7 µm [$L_m \times W_m$ = 2.7–4.3 × 1.5–2.0], thin-walled, hyaline. ***Cells at lamella edge*** [60/7/6] 19.4–53.3 × 9.4–31.6 µm [$L_m \times W_m$ = 23.4–43.3 × 10.5–20.6 µm], appeared globose–subglobose or pyriform, but basically pyriform, clavate, or spatulate (Supplementary Fig. S7), thin-walled, hyaline. ***Elements of annulus*** mostly composed of filamentous hyphae; hyphae 2–8 µm in diam, smooth, thin-walled or sometimes thick-walled, hyaline or sometimes thromboplerous-like, clamp connection present; thromboplerous-like hyphae 2–3 µm in diam; inflated cells 30–80 × 10–20 µm, subglobose to oblong, smooth, thin-walled, hyaline, rare (Supplementary Fig. S8). ***Elements of volva*** mostly composed of filamentous hyphae; hyphae 2–10 µm in diam, smooth, thin-walled or often thick-walled, hyaline or sometimes thromboplerous-like, clamp connection present; inflated cells (30–60 × 20–40 µm) present on the outer surface but not on the inner surface.

Ecology: Under temperate–subtropical forests, dominated by *Quercus serrata*, *Quercus glauca*, *Quercus acutissima*, *Castanopsis sieboldii*, *Fagus crenata*, *Betula platyphylla* var. *japonica*, *Pinus densiflora*, *Tsuga sieboldii*, and *A. firma*. Fruiting season in Jun to Oct.

Known distribution: Japan, from the southwest of Hokkaido Island as the northern limit to Okinawa Island as the southern limit.

Additional specimens examined in Japan: Hokkaido Pref., S-257 (= TNS-F-61979; N. Endo); Aomori Pref., AC-24-2 (M. Kodaira); Gunma Pref., AC-37-2 (R. Nagumo); Niigata Pref., AC-41-2 (M. Kodaira); Nagano Pref., AC-32 (R. Nagumo), AC-70-5 (M. Kodaira), AC-43-1 (M. Kodaira), AC48 (M. Kodaira), Okaya201108 (A. Yamada), AC-23 (A. Yamada), AC-34-1 (M. Kodaira), AC-35-3 (M. Kodaira), Ahem080927 (N. Endo), AC-28-2 (M. Kodaira), AC-30 (M. Kodaira), AC-45 (M. Kodaira), 2070921Y (N. Endo), S-108 (= TNS-F-61969; N. Endo), Ahem080907 (= TNS-F-61982; N. Endo); Yamanashi Pref., AC-39-4 (M. Kodaira); Tokyo Metropolis, S-325 (N. Endo), S-327 (= TNS-F-61983; N. Endo); Shiga Pref., Hongo 5297 (= OSA-MY100271; T. Hongo); Wakayama Pref., AC-14-1 (M. Kodaira), AC-17 (M. Kodaira); Tottori Pref., AC-22 (N. Endo); Oita Pref., S-78 (A. Hadano); Miyazaki Pref., S-70 (T. Katayama); Okinawa Pref., Mar20170515-01 (N. Endo).

Commentary: Most specimens of *A. satotamagotake* correspond to *A. hemibapha* sensu Hongo (Hongo, 1975, 1982; Imazeki & Hongo, 1987) in their macromorphology and the shape and size of basidiospores. Basidiospores of *A. satotamagotake* were significantly smaller than basidiospores of *A. caesareoides* when their mean values were compared at the population level (Table 5). Therefore, it is difficult to distinguish *A. caesareoides* (Supplementary Fig. S6) from *A. satotamagotake* based on morphological characteristics. The hyphal cells of the pileus (pileipellis and trama), lamella, annulus, stipe (outer and inner), and volva (outer and inner) were similar between *A. caesareoides* and *A. satotamagotake*. Clamp connections were observed on the hyphae in all these tissues. Differences were observed only in the annulus cells. Inflated cells (globose–subglobose–pyriform) tended to be larger in *A. caesareoides* than in *A. satotamagotake*. In addition, *A. caesareoides* showed inflated gloeoplerous or thromboplerous hyphae (>10 µm in diam), but *A. satotamagotake* showed narrow thromboplerous hyphae (2–3 µm in diam). However, due to the limited number of specimens available for microscopic observation of the annulus, we did not use these morphological characters for taxonomic distinction.

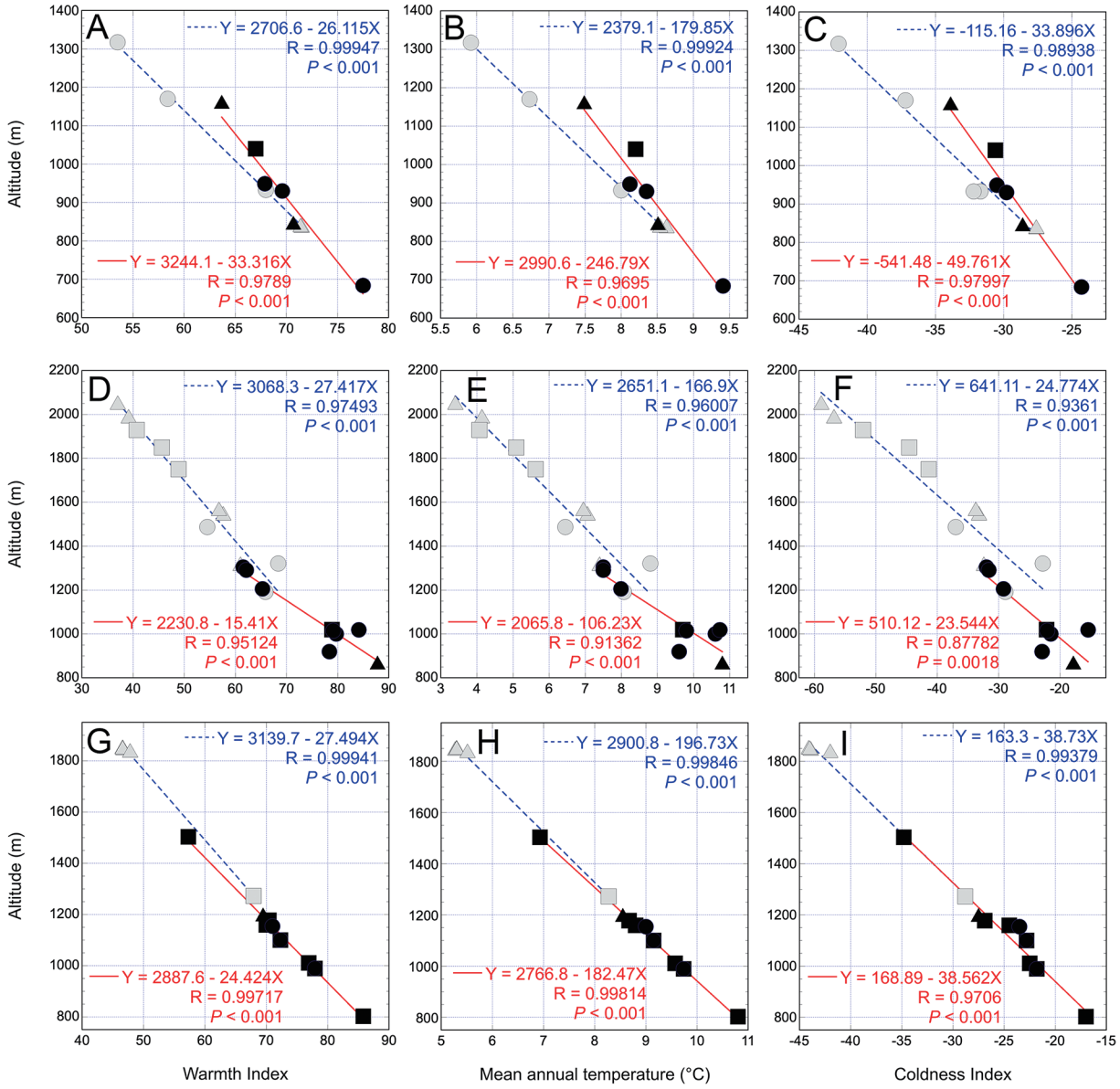

Fig. 9 – Vertical distribution patterns of two *Amanita caesareoides* populations (HE and LE) in relation to warmth index (WI; A, D, G), mean annual temperature (MAT; B, E, H), and coldness index (CI; C, F, I) in the Myoko Volcano Group (A–C), Yatsugatake Mountains and marginal ranges (D–F), and Ina Mountains and the marginal ranges of the Akaishi Mountains (G–I). Open and closed symbols, sampling sites of HE and LE populations, respectively. Triangle, conifer forest; square, mixed forest; circle, broad-leaf forest (oak or birch). Regression lines are shown for the HE (dotted, blue) and LE (solid, red) populations.

In contrast, phylogenetic data (IGS1 of nuc rDNA, *RPB2*, *TEF1*, *COX3*, and *ATP6*), geographic distribution (habitat), and culture characteristics show substantial differences between *A. satotamagotake* and *A. caesareoides*, and no intermediate specimens were found. As the type specimen AC-36 showed a macroscopically younger trend (Fig. 9), we evaluated spore maturity. However, basidiospores were fully developed and the measured size was ordinary in the *A. satotamagotake* specimens (Supplementary Table S6).

Amanita caesarea and *A. jacksonii*, red and orange pileal Caesar's mushrooms related to *A. caesareoides*, were morphologically distinguishable from *A. satotamagotake*; *A. caesarea* is distinguished from *A. satotamagotake* by the non-umbonate pileus and larger and more elongated spores (Supplementary Table S6; Neville & Poumarat, 2004). *Amanita jacksonii* is similar to *A. satotamagotake* in macromorphology, but it has more elongated spores (Supplementary Table S6; Guzmán & Ramírez-Guillén, 2001; Tulloss & Yang, 2009). *Amanita subhemibapha* and *A. rubroflava*, both of which are yellow- to reddish-pileal species in the section *Caesareae* recently described from China (Cui et al., 2018), are similar to *A. satotamagotake* in terms of spore size (Supplementary Table S6). However, *A. subhemibapha* has a non-umbonate pileus, whereas *A. satotamagotake* has an umbonate pileus. *Amanita rubroflava* shows a distinct color gradient on the pileal surface (from red in the center to yellow in the margin), whereas *A. satotamagotake* has an evenly reddish or orangish pileal surface. Both Chinese species had phylogenetic positions distinct from the *A. satotamagotake* and *A. caesareoides* clades (Figs. 2–4).

The lamella edge was occupied by unique inflated cells, and no basidia were observed there (Fig. 11L, M). As these inflated cells (pyriform, clavate, or spatulate in overall shape including the base) were the terminal cells of the lamella trama (Supplementary Fig.

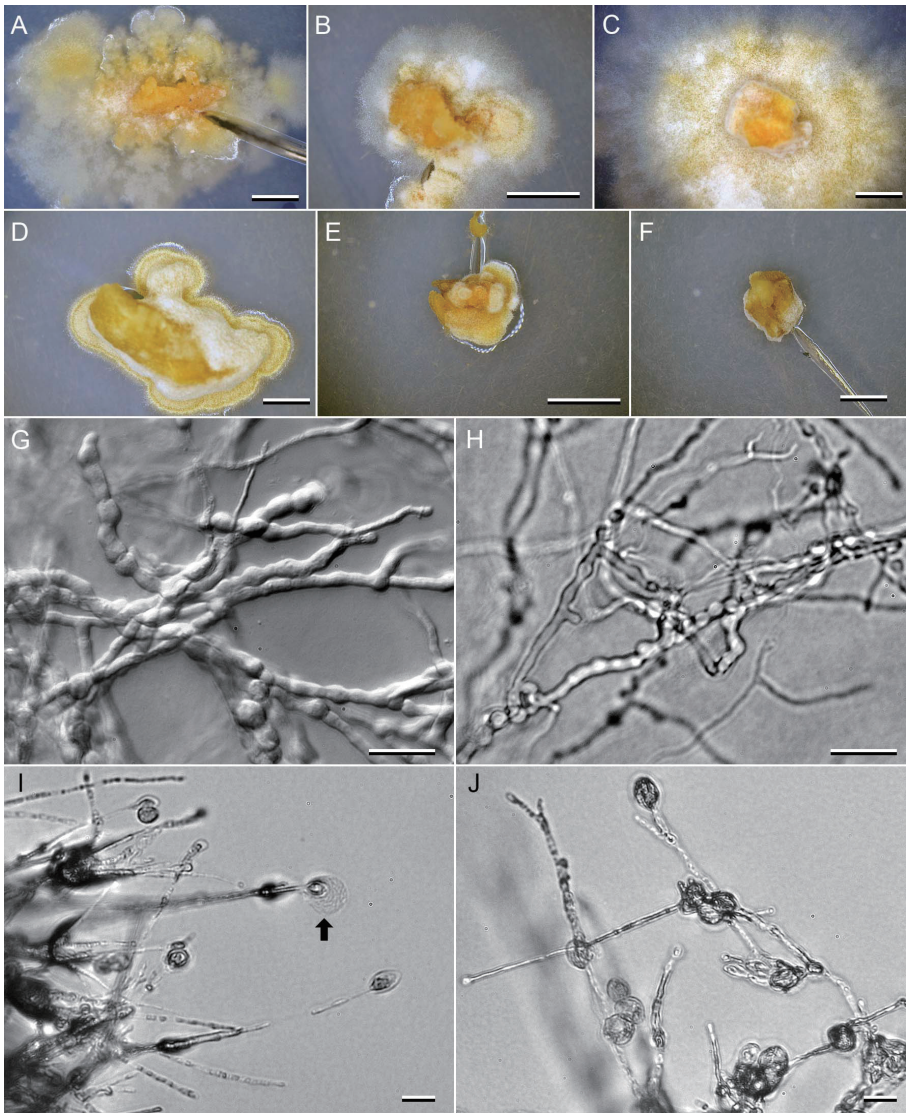

Fig. 10 – Cultured mycelia of *Amanita caesareoides* HE and LE populations on MNC agar. A–F, Colony morphology under a dissecting microscope. A–C, AC-8, AC-47 and AC-67-1 (all HE populations); D–F, AC-26, AC-66-11, and AC-70-1 (all LE population). G–J, hyphal structure under a light microscope; G, monilioid cell-like hyphae on the surface of MNC agar in AC-47; H, submerged hyphae with monilioid cell-like enlargement in AC-67-1; I, aerial hyphae with terminal enlargement in AC-66-11, some of which have ruptured, on MNC agar (arrow); J, aerial hyphae with terminal enlargement in AC-70-1. *Bars*: A–F 5 mm; G–J 20 μm.

Table 5. Statistic comparisons of morphological characteristics between two populations of *Amanita caesareoides*.

Measured parameter	HE population (phylogroup A)			LE population (phylogroup B)			*P*-value (t-test)
	N	Mean	SE	N	Mean	SE	
(Cultured mycelium)							
Colony area (mm²)	6	215.2	38.5	12	20.2	3.7	< 0.0001
Cultured hyphal width (μm)	5	3.22	0.16	8	3.51	0.18	0.285
Length of terminal swelling of cultured hyphae (μm)	5	(absent)		8	22.6	1.3	(Not determined)
Width of terminal swelling of cultured hyphae (μm)	5	(absent)		8	14.0	1.2	(Not determined)
(Basidioma)							
Spore length (μm)	26	8.91	0.08	29	8.33	0.06	< 0.0001
Spore width (μm)	26	7.38	0.07	29	7.00	0.06	< 0.0001
L/W ratio of spore	26	1.21	0.01	29	1.20	0.01	0.177
Basidium length (μm)	15	44.4	0.8	14	43.8	0.9	0.614
Basidium width (μm)	15	10.5	0.2	14	10.5	0.2	0.950
Sterigma length (μm)	18	3.95	0.15	18	3.56	0.14	0.0579
Sterigma width (μm)	18	1.79	0.07	18	1.72	0.04	0.301
Length of cheilocystidium-like inflated cell (μm)	9	32.4	0.9	14	33.3	1.9	0.698
Width of cheilocystidium-like inflated cell (μm)	9	16.4	0.8	14	17.0	1.0	0.688

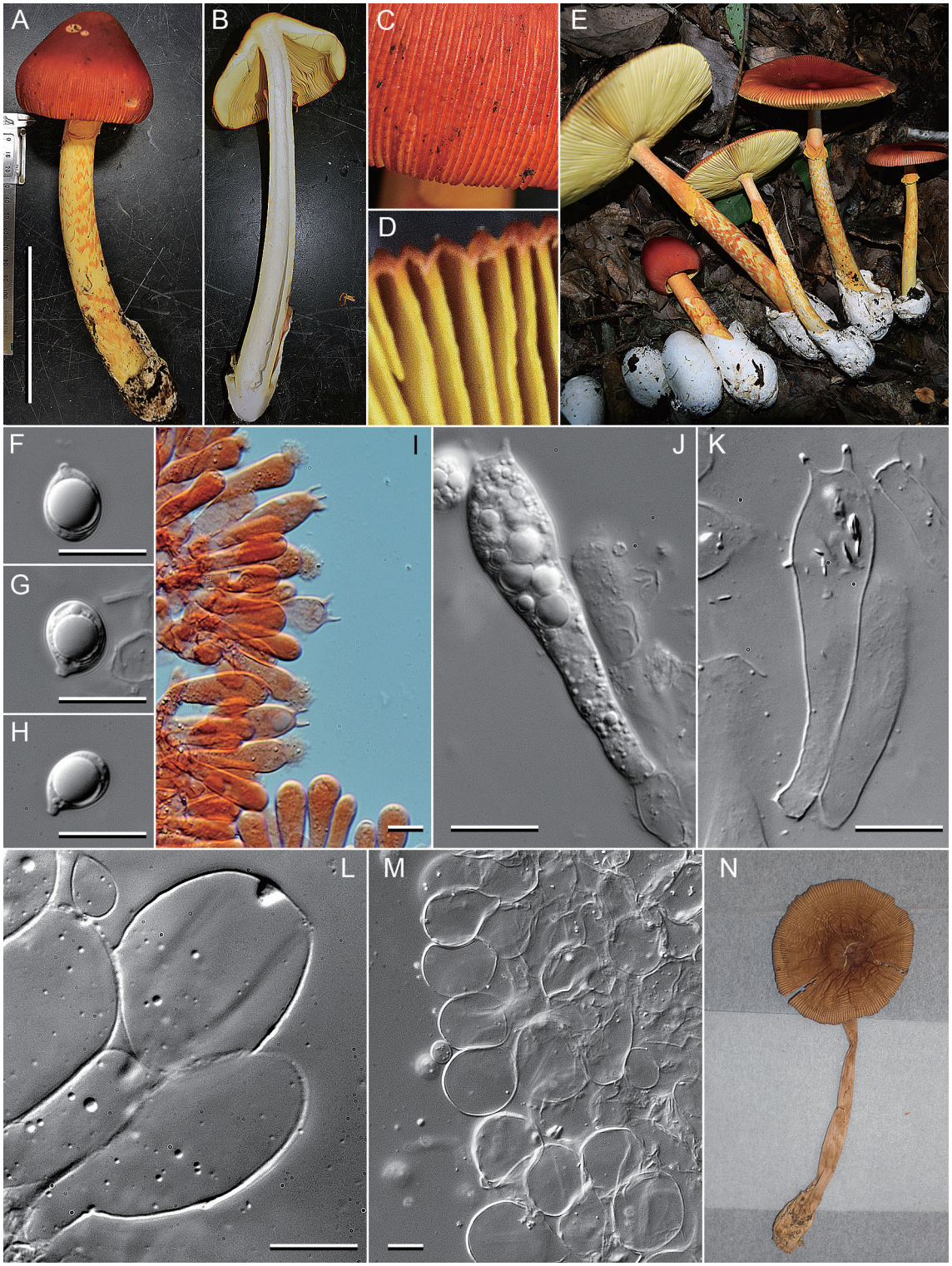

Fig. 11 – Macro- and microscopic characteristics of *Amanita satotamagotake*. A–D: External morphology of a basidioma (A), sectioned view (B), stria on the pileal margin (C), and yellowish lamellae with reddish margin at the boundary with the stria (D) of specimen AC-36 (holotype). E, Growth of mature and young basidiomata of specimen AC-70-5. F–L: Basidiospores (F–H), basidia (I–K), and cells on the lamella edge (L) of AC-36. M, Cells on the lamella edge of AC-28-2. N, External morphology of a basidioma of Hongo 5297. *Bars*: A 10 cm; F–M 10 μm.

S7), they can be considered cheilocystidia (Clémençon et al., 2011).

5. Discussion

The Japanese reddish-pileus Caesar's mushroom consists of two species, *A. caesareoides* and *A. satotamagotake*, based on the concatenated six-locus phylogenetic tree (Fig. 5), although they have long been regarded as a single species (Endo, 2015; Endo et al., 2016; Hennings, 1900; Hongo, 1975, 1982; Imazeki & Hongo, 1987; Kawamura, 1913, 1954). They converged in a single clade in the ITS

phylogeny (Fig. 2), although the statistical independency was insufficient. Notably, the two species are difficult to distinguish based on morphological characteristics. Phylogenetic trees of *β-TUB*, *RPB2*, *TEF1*, *ATP6*, and *COX3* (Figs. 3 and 4; Supplementary Figs. S1–S3) revealed minimal topological differences between *A. caesareoides* (= phylogroup A) and *A. satotamagotake* (= phylogroup B). Such phylogenetic relationships enabled estimation of the divergence time between these two species in relation to their closest relatives, *A. jacksonii* and *A. caesarea*. Sánchez-Ramírez et al. (2015a) used a Japanese reddish-pileus Tamagotake specimen included in *A. satotamagotake*, but they did not use any specimens of *A. caesareoides*. As *A. satotamagotake* is closer to *A. jacksonii* (Fig. 5), the previously estimated divergence time of around 6–8 Mya (Sánchez-Ramírez et al., 2015a) is reasonable. However, the notion of divergence of *A. caesarea* directly from the ancestral lineage of section *Caesareae* in the southeastern–southwestern Asian region (Sánchez-Ramírez et al., 2015a) should be reconsidered because our data indicated that *A. caesarea*, in parallel with *A. caesareoides*, diverged from *A. satotamagotake*, presumably in eastern Asia at 2.38–7.54 Mya (Fig. 6). This divergence issue will presumably be resolved by examining *A. caesareoides* specimens from Siberia and from the expected *A. caesareoides–A. caesarea* continuum in central Eurasia (e.g., western Russia and north-central Asia).

Phylogenetic analyses of nuclear and mitochondrial DNA regions indicated that there were no hybrids between *A. caesareoides* and *A. satotamagotake* in the Japan islands. This finding suggests that the two populations show reproductive isolation even if both species are sympatrically present and concurrently developed fruiting bodies in the same forest site. Indeed, the lakesides of Reisenji-ko, Matsubara-ko, and Komade-ike harbored both species. Notably, in the lakesides of Reisenji-ko and Komade-ike, *A. satotamagotake* fruited in the warmer season (late summer) and *A. caesareoides* fruited in the cooler season (early summer or autumn) (Table 2; Supplementary Table S2). Although these distinct fruiting periods suggest a mechanism for reproductive isolation, both species fruited in late summer at Matsubara-ko. Therefore, there must be a more robust genetic mechanism for reproductive isolation. As mating-factor genes control cell fusion and the subsequent nuclear transfer events (Moor et al., 2020), genetic analyses of these loci are needed. Reproductive isolation has been examined in cultivated mushrooms by crossbreeding experiments (e.g., de Mattos-Shipley et al., 2016). However, it is difficult to perform mating tests with Caesar's mushrooms. Indeed, homokaryotic (monokaryotic) mycelial culture isolation has not yet been reported for Caesar's mushrooms, and most established cultures of *A. caesarea* and *A. caesareoides* are dikaryotic (Daza et al., 2006; Endo, 2015; Endo et al., 2013). Analysis of the nuc rDNA IGS1 region showed limited phylogenetic distinction between *A. caesareoides* and *A. satotamagotake*, but indicated that their tandem repeats have different structures, i.e., direct sequencing is possible in *A. caesareoides* but cloning is required in *A. satotamagotake* because of numerous mutations (Supplementary Fig. S4). Indeed, 34 point mutations were detected in the IGS1 region of *A. satotamagotake* specimen S-70, and 3–4 cytosine insertions were detected at nucleotides 518–521 in the 1003-bp alignment of nine cloned sequences (data not shown).

The present phylogenetic data suggest that the ITS region of nuc rDNA is not capable of discriminating cryptic species of Caesar's mushrooms, despite its usefulness in DNA barcoding of diverse fungal taxa at the species level; this discrepancy has also been reported for *Hebeloma* (Aanen et al., 2000; Eberhardt et al., 2015; Vesterholt et al., 2014), *Serpula* (Balasundaram et al., 2015), and *Tricholoma* (Aoki et al., 2022). It is difficult to separate recently diverged species on a geochronological age scale (e.g., 2.6–10.6 Mya) by ITS phylogeny, which may incorrectly group cryptic species (Ryberg, 2015; Ryberg & Matheny, 2012). Based on the general trend of ITS phylogeny, the estimated divergence time of around 2.81–7.54 Mya for *A. satotamagotake* and *A. caesareoides* by the consensus phylogeny of seven loci can therefore be regarded as plausible, but the divergence times of around 6–8.48 Mya for *A. jacksonii* and *A. satotamagotake*, and 0.8–4.02 Mya for *A. caesarea* and *A. caesareoides* are not plausible. The discrepancy between the general trend of ITS sequence evolution and the estimation of evolutionary pattern among closely related taxa by multi-gene analysis suggests that the latter approach can provide insight into the evolution of Caesar's mushroom.

We discovered physiological differences between *A. satotamagotake* and *A. caesareoides*; only colony mycelia of *A. caesareoides* could be subcultured on MNC agar. Notably, all Tamagotake isolates (S-46, S-48, S-125, S-248) reported as *A. caesareoides* based on the ITS sequence (Endo, 2015; Endo et al., 2013) were identified as *A. caesareoides*; no isolate was identified as *A. satotamagotake*. In addition, colony morphology and related hyphal structure differed between these two species. The probable differences in nutrient requirement between these two species suggest substantial differences in ecophysiological properties. As the subculture of *A. satotamagotake* mycelia on MNC agar failed, we could not compare the optimal temperatures for mycelial growth. We suspect that *A. caesareoides* and *A. satotamagotake* mycelia have different optimal growth temperatures because of the different climates in which they are distributed. As we cultivated *A. caesareoides* at 20 °C–25 °C, *A. satotamagotake* may show better growth at > 25 °C.

There were no distinct macromorphological differences between *A. caesareoides* and *A. satotamagotake*, although *A. caesareoides* tended to have larger basidiomata and greater variation in stipe ornamentation (Supplementary Fig. S7). The only distinguishable morphological characters at the population level were spore size and sterigma length (smaller in *A. satotamagotake* than in *A. caesareoides*), suggesting that *A. satotamagotake* is a truly cryptic species relative to *A. caesareoides*. Similar cases of morphologically non-distinguishable cryptic Caesar's mushroom species have been reported from North America; 10 and 9 species are phylogenetically distinguished in the *A. jacksonii* and *A. basii* clades, respectively (Sánchez-Ramírez et al., 2015b). In the former *A. jacksonii* clades, nine undescribed species have been suggested. In other mushroom taxa, the *Suillus pictus–Suillus phylopictus* relationship (Zhang et al., 2017) and the two phylogenetically distinguishable populations of *Tricholoma matsutake* in Eurasia (i.e., B/C and A/E clades; Aoki et al., 2022) are also suggested to be cryptic. The first report of Tamagotake under the name "*A. caesarea*" based on macroscopic data (Kawamura, 1913) with supportive microscopic data (Kawamura, 1954) was presumably *A. caesareoides* based on its morphological characteristics, habitat properties, and fruiting phenology. The first report of "*A. caesarea*" from Japan (Hennings, 1900) was also presumably *A. caesareoides* based on its macroscopic characteristics (crimson type; Shirai & Hennings, 1899) and habitat (WI 56.2; Supplementary Table S1). In *A. hemibapha* sensu Hongo (Hongo, 1975, 1982), the partial *TEF1* sequence of the Hongo 5297 specimen and other *A. satotamagotake* specimens, including holotype AC-36, showed 100% similarity (Table 4), suggesting that Hongo 5297 is *A. satotamagotake*; this was confirmed by the habitat data (WI 119.7). Considering these taxonomic histories, the Hongo 5297 specimen could be a holotype of *A. satotamagotake*. As DNA degradation hindered full phylogenetic analysis of this specimen, no such designation was assigned.

Amanita satotamagotake and *A. caesareoides* are distributed in different climatic regions (Fig. 7; Supplementary Fig. S5). However,

several forest sites harbored both species in the central Japanese Archipelago, such as Mt. Madarao-yama and the lakesides of Reisenji-ko and Komade-ike, where the WI values were 68–69.5, 70.7–71.5, and 61–62.1, respectively (Supplementary Table 1). This suggests that both species are sympatrically present and possibly competitive at the forest sites, but there is no hybridization in terms of interspecific crossing. The minimum WI values in *A. satotamagotake* habitats were 57.3 at Mt. Togurayama (AC-45) and 58.0 at Mikuni-touge pass (AC-37-2), where *A. caesareoides* was strongly expected to be naturally present because of these lower WI values. In contrast, the maximum WI values in *A. caesareoides* habitats were 70.9 at the lakeside of Reisenji-ko, Iizuna, Nagano (AC-66-1), 68.0 at Mt. Madarao-san, Iiyama, Nagano, (AC-72-1, AC-72), and 67.9 at Fujisawa, Ina, Nagano (AC-28-2). Therefore, areas with WI values of 57–71 may harbor both *A. satotamagotake* and *A. caesareoides*. As Mt. Togurayama in Nagano and Mikuni-touge pass in Gunma lacked subalpine–cool temperate conifer vegetation in high-elevation areas, *A. caesareoides* might have ceased occupation of those areas, leading to occupation by *A. satotamagotake* that ascended from low-elevation areas. *Amanita caesareoides* is often associated with conifers in high-elevation (and lower WI) areas. These data suggest that the different geographic distributions of *A. satotamagotake* and *A. caesareoides* are primarily determined by temperature and secondarily determined by forest vegetation. Similarly, large-scale analyses of soil ectomycorrhizal fungi suggested that temperature (MAT) and vegetation are important (van der Linde et al., 2018; Miyamoto et al., 2018).

Our analysis of the effect of temperature on fungal habitat and distribution suggested the advantage of adopting WI, rather than MAT and CI (Fig. 7; Supplementary Fig. S5). Therefore, we compared the distribution patterns of *A. satotamagotake* and *A. caesareoides* within a geographically restricted area in relation to WI. In the Myoko Volcano Group, Yatsugatake Mountains, and Ina Mountains and the marginal ranges of the Akaishi Mountains, *A. satotamagotake* and *A. caesareoides* exhibited different vertical distributions (Figs. 8, 9). In the Myoko Volcano Group, the habitats of these two species overlapped at approximately 800–1200 m. However, in the overlap region, the two species showed different WI trend; at the same elevation, *A. satotamagotake* and *A. caesareoides* preferred sites with high and low WI values, respectively. These findings suggest that, at the same elevation, *A. satotamagotake* prefers open forest sites or southern slopes, whereas *A. caesareoides* prefers closed forest sites or northern slopes. If the WI value were to increase by 5–10, the habitat of *A. caesareoides* would retreat to areas of approximately 100–200 m asl, and the habitat of *A. satotamagotake* would expand into that area. In addition, if land use changed from deep forest (canopy closure) to open forest, the area of *A. caesareoides* habitat would presumably decrease because of excess irradiation and an increased WI value.

Based on the scenario described above, the geographically isolated *A. satotamagotake* specimens (specimens S-257 and S-320) at Atsubetsu, Sapporo on Hokkaido Island may have invaded or been artificially introduced from Honshu Island and subsequently established a habitat (WI 70.1). Thus, global warming may decrease the area of *A. caesareoides* habitat and lead to replacement with *A. satotamagotake*. As WI has been increasing by approximately 5–15/century because of the increasing annual mean temperature since the beginning of the 20th century in temperate areas of the Japanese Archipelago (Supplementary Table S7), forests in the southern coastal region of Hokkaido may alternate from *A. caesareoides* to *A. satotamagotake*. The distributions of many terrestrial organisms are shifting in latitude or elevation in response to climate change (Chen et al., 2011), but for ectomycorrhizal fungi, there is little data on the rate and magnitude of habitat and distribution changes with global warming (Bidartondo et al., 2018). In forest trees including ectomycorrhizal species, northward tree migration in the eastern United States is underway at rates approaching 100 km/century for many species (Woodall et al., 2009). The differences in habitat among cryptic species of Caesar's mushroom observed in this study will enable investigation of these environmental issues. Conservation of fungal diversity requires an accurate taxonomy of similar cryptic species.

Declaration of competing interests

The authors of this study have no conflicts of interest to declare.

Acknowledgement

We thank the staff of the Research Center for Human and Environmental Sciences, Shinshu University for the DNA sequencing. This study was supported in part by a Grant-in-Aid for Scientific Research (15H01751) from the Ministry of Education, Culture, Sports, Science, and Technology of Japan.

References

Aanen, D. K., Kuyper, T. W., Boekhout, T., & Hoekstra, R. F. (2000). Phylogenetic relationships in the genus *Hebeloma* based on ITS1 and 2 sequences, with special emphasis on the *Hebeloma crustuliniforme* complex. *Mycologia*, *92*, 269–281. https://doi.org/10.2307/3761560

Anderson, J. B., & Stasovski, E. (1992). Molecular phylogeny of Northern hemisphere species of *Armillaria*. *Mycologia*, *84*, 505–516. http://doi.org/10.2307/3760315

Anisimova, M., Gil, M., Dufayard, J. F., Dessimoz, C., & Gascuel, O. (2011). Survey of branch support methods demonstrates accuracy, power, and robustness of fast likelihood-based approximation schemes. *Systematic Biology*, *60*, 685–699. http://doi.org/10.1093/sysbio/syr041

Aoki, W., Bergius, N., Kozlan, S., Fukuzawa, F., Okuda, H., Murata, H., Ishida, T. A., Vaario, L.-M., Kobayashi, H., Kalmiş, E., Fukiharu, T., Gisusi, S., Matsushima, K., Terashima, Y., Narimatsu, M., Matsushita, N., Ka, K.-H., Yu, F., Yamanaka, T., Fukuda, M., & Yamada, A. (2022). New findings on the fungal species *Tricholoma matsutake* from Ukraine, and revision of its taxonomy and biogeography based on multilocus phylogenetic analyses. *Mycoscience*, *63*, 197–214. http://doi.org/10.47371/mycosci.2022.07.004

Balasundaram, S. V., Engh, I. B., Skrede, I., & Kauserud, H. (2015). How many DNA markers are needed to reveal cryptic fungal species? *Fungal Biology*, *119*, 940–945. https://doi.org/10.1016/j.funbio.2015.07.006

Bidartondo, M. I., Ellis, C. Kauserud, H., Kennedy, P. G., Lilleskov, E., Suz, L. M., & Andrew, C. (2018). Chapter 9. Climate change: fungal responses and effects. In: K. J. Willis (ed.), *State of the World's Fungi 2018* (pp. 62–69). Royal Botanical Gardens, Kew. https://www.fs.usda.gov/nrs/pubs/jrnl/2018/nrs_2018_bidartondo_001.pdf

Chen, I.-C., Hill, J. K., Ohlemüller, R., Roy, D. B., & Thomas, C. D. (2011). Rapid range shifts of species associated with high levels of climate warming. *Science*, 333, 1024–1026. https://doi.org/10.1126/science.1206432

Cho, H. J., Park, M. S., Lee, H., Oh, S. Y., Jang, Y., Fong, J. J., & Lim, Y. W. (2015). Four new species of *Amanita* in Inje County, Korea. *Mycobiology*, *43*, 408–414. https://doi.org/10.5941/MYCO.2015.43.4.408

Clémençon, H., Emmett, V., & Emmett, E. E. (2011) *Cytology and plectology of the hymenomycetes, 2nd edn. (Bibliotheca Mycologica Volume: 199)*. J. Cramer Verlag.

Cohen, K. M., Finney, S. C., Gibbard, P. L., & Fan, J-X. (2013). The ICS international chronostratigraphic chart. *Episodes*, *36*, 199–204. https://stratigraphy.org/ICSchart/Cohen2013_Episodes.pdf

Cui, Y. Y., Cai, Q., Tang, L. P., Liu, J. W., & Yang, Z. L. (2018). The family Amanitaceae: molecular phylogeny, higher-rank taxonomy and the species in China. *Fungal Diversity*, *91*, 5–230. https://doi.org/10.1007/s13225-018-0405-9

Daza, A., Manjón, J. L., Camacho, M., De La Osa, L. R., Aguilar, A., & Santamaría, C. (2006). Effect of carbon and nitrogen sources, pH and temperature on in vitro culture of several isolates of *Amanita caesarea* (Scop.:Fr.) Pers. *Mycorrhiza, 16,* 133–136. https://doi.org/10.1007/s00572-005-0025-6.

de Mattos-Shipley, K. M. J., Ford, K. L., Alberti, F., Banks, A. M., Bailey, A. M., & Fos-

ter, G. D. (2016). The good, the bad and the tasty: The many roles of mushrooms. *Studies in Mycology, 85,* 125–157. https://doi.org/10.1016/j.simyco.2016.11.002

Drummond, A. J., & Bouckaert, R. R. (2015). Bayesian evolutionary analysis with BEAST. Cambridge University Press. https://doi.org/10.1017/CBO9781139095112

Duchesne, L. C., & Anderson, J. B. (1990). Location and direction of transcription of the 5S rRNA gene in *Armillaria*. *Mycological Research*, *94*, 266–269. https://doi.org/10.1016/S0953-7562(09)80626-6

Eberhardt, U., Beker, H. J., & Vesterholt, J. (2015). Decrypting the *Hebeloma crustuliniforme* complex: European species of *Hebeloma* section *Denudata* subsection *Denudata* (*Agaricales*). *Persoonia*, *35*, 101–147. https://doi.org/10.3767/003158515X687704

Edgar, R. C. (2004). MUSCLE: a multiple sequence alignment method with reduced time and space complexity. *BMC Bioinformatics*, *5*, 113. https://doi.org/10.1186/1471-2105-5-113

Endo, N. (2015). *Cultivation studies in the edible Caesar's mushrooms* "Tamagotake" *(*Amanita caesareides *and its relatives)* [in Japanese]. [PhD dissertation, Shinshu University].

Endo, N., Fangfuk, W., Kodaira, M., Sakuma, D., Hadano, E., Hadano, A., Murakami, Y., Phosri, C., Matsushita, N., Fukuda, M., & Yamada, A. (2017). Reevaluation of Japanese *Amanita* section *Caesareae* species with yellow and brown pileus with descriptions of *Amanita kitamagotake* and *A. chatamagotake* spp. nov. *Mycoscience*, *58*, 457–471. https://doi.org/10.1016/j.myc.2017.06.009

Endo, N., Fanfuk, W., Sakuma, D., Phosri, C., Matsushita, N., Fukuda, M., & Yamada, A. (2016). Taxonomic consideration of the Japanese red-cap Caesar's mushroom based on morphological and phylogenetic analyses. *Mycoscience*, *57*, 200–207. https://doi.org/10.1016/j.myc.2016.01.005

Endo, N., Gisusi, S., Fukuda, M., & Yamada, A. (2013). In vitro mycorrhization and acclimatization of *Amanita caesareoides* and its relatives on *Pinus densiflora*. *Mycorrhiza*, *23*, 303–315. https://doi.org/10.1007/s00572-012-0471-x

Gardes, M., & Bruns, T. D. (1993). ITS primers with enhanced specificity for basidiomycetes: application to the identification of mycorrhizae and rusts. *Molecular Ecology*, *2*, 113–118. http://doi.org/10.1111/j.1365-294X.1993.tb00005.x

Guindon, S., Dufayard, J.-F., Lefort, V., Anisimova, M., Hordijk, W., & Gascuel, O. (2010). New algorithms and methods to estimate maximum-likelihood phylogenies: assessing the performance of PhyML 3.0. *Systematic Biology*, *59*, 307–321. http://doi.org/10.1093/sysbio/syq010

Guzmán, G., & Ramírez-Guillén, F. (2001). *The Amanita caesarea-complex. (Bibliotheca Mycologica 187).* J Cramer.

Hayatsu, K., Shimizu, S., & Itaya, T. (1994). Volcanic history of Myoko volcano group, central Japan –poly-generation volcano–. *Journal of Geography*, *103*, 207–220. https://www.jstage.jst.go.jp/article/jgeography1889/103/3/103_3_207/_pdf

Hennings, P. (1900). Fleischige Pilze aus Japan. *Hedwigia Beiblatt, 39*, 155–157. https://www.zobodat.at/pdf/Hedwigia_Beiblatt_39_1900_0155-0157.pdf

Hongo, T. (1975). Notulae Mycologicae 14. *Memories of the Faculty of Education Shiga University Natural Science*, *25*, 56–63.

Hongo, T. (1982). The *Amanitas* of Japan. *Acta Phytotaxonomica et Geobotanica*, *33*, 116–126. https://doi.org/10.18942/bunruichiri.KJ00001079145

Imazeki, R., & Hongo, T. (1987). *Colored illustrations of mushrooms of Japan I* [in Japanese]. Hoikusha.

Kalyaanamoorthy, S., Minh, B. Q., Wong, T. K. F., von Haeseler, A., & Jermiin, L. S. (2017). ModelFinder: fast model selection for accurate phylogenetic estimates. *Nature Methods*, *14*, 587–589. http://doi.org/10.1038/nmeth.4285

Kawamura, S. (1913). *Illustrations of Japanese fungi, 2nd del* [in Japanese]. The Bureau of Forestry, Ministry of Agriculture and Commerce.

Kawamura, S. (1930). *The Japanese Fungi* [in Japanese]. Daichi-shoin.

Kawamura, S. (1931). *Edible and poisonous mushrooms* [in Japanese]. Iwanami-shoten.

Kawamura, S. (1954). *Icons of Japanese fungi* [in Japanese]. Kazama-shobo.

Kira, T. (1948). On the altitudinal arrangement of climate zones in Japan: a contribution to the rational land utilization in cool highlands [in Japanese]. *Agricultural Science of the North Temperate Region*, *2*, 143–173.

Kohler, A., Kuo, A., Nagy, L. G., Morin, E., Barry, K. W., Buscot, F., Canbäck, B., Choi, C., Cichocki, N., Clum, A., Colpaert, J., Copeland, A., Costa, M. D., Doré, J., Floudas, D., Gay, G., Girlanda, M., Henrissat, B., Herrmann, S., Hess, J., Högberg, N., Johansson, T., Khouja, H. R., LaButti, K., Lahrman,n U., Levasseur, A., Lindquist, E. A., Lipzen, A., Marmeisse, R., Martino, E., Murat, C., Ngan, C. Y., Nehls, U., Plett, J. M., Pringle, A., Ohm, R. A., Perotto, S., Peter, M., Riley, R., Rineau, F., Ruytinx, J., Salamov, A., Shah, F., Sun, H., Tarkka, M., Tritt, A., Veneault-Fourrey, C., Zuccaro, A., Mycorrhizal Genomics Initiative Consortium, Tunlid, A., Grigoriev, I. V., Hibbett, D. S., & Martin, F. (2015). Convergent losses of decay mechanisms and rapid turnover of symbiosis genes in mycorrhizal mutualists. *Nature Genetics*, *47*, 410–415. https://doi.org/10.1038/ng.3223

Kretzer, A. M., & Bruns, T. D. (1999). Use of *ATP6* in fungal phylogenetics: an example from the Boletales. *Molecular Phylogenetics and Evolution*, *13*, 483–492. https://doi.org/10.1006/mpev.1999.0680

Kumar, S., Stecher, G., & Tamura, K. (2016). MEGA7: molecular evolutionary genetics analysis version 7.0 for bigger datasets. *Molecular Biology and Evolution*, *33*, 1870–1874. https://doi.org/10.1093/molbev/msw054

Lanfear, R., Calcott, B., Ho, S. Y. W., & Guindon, S. (2012). PartitionFinder: Combined selection of partitioning schemes and substitution models for phylogenetic analyses. *Molecular Biology and Evolution*, *29*, 1695–1701. https://doi.org/10.1093/molbev/mss020

Lanfear, R., Frandsen, P. B., Wright, A. M., Senfeld, T., & Calcott, B. (2017). PartitionFinder 2: new methods for selecting partitioned models of evolution for molecular and morphological phylogenetic analyses. *Molecular Biology and Evolution*, *34*, 772–773. https://doi.org/10.1093/molbev/msw260

Matheny, P. B. (2005). Improving phylogenetic inference of mushrooms with *RPB1*and *RPB2* nucleotide sequences (*Inocybe*; Agaricales). *Molecular Phylogenetics and Evolution, 35*, 1–20. https://doi.org/10.1016/j.ympev.2004.11.014

Matsumura, J. (1904). *Index plantarum japonicum I. Cryptogamae*. Maruzen.

Minh, B. Q., Nguyen, M. A. T., & Haeseler, A. (2013). Ultrafast approximation for phylogenetic bootstrap. *Molecular Biology and Evolution, 30*, 1188–1195. http://doi.org/10.1093/molbev/mst024

Miyamoto, Y., Terashima, Y., & Nara, K. (2018). Temperature niche position and breadth of ectomycorrhizal fungi: Reduced diversity under warming predicted by a nested community structure. *Global Change Biology*, *24*, 5724–5737. https://doi.org/10.1111/gcb.14446

Morehouse, E. A., James, T. Y., Ganley, A. R., Vilgalys, R., Berger, L., Murphy, P. J., & Longcore, J. E. (2003). Multilocus sequence typing suggests the chytrid pathogen of amphibians is a recently emerged clone. *Molecular Ecology*, *12*, 395–403. https://doi.org/10.1046/j.1365-294X.2003.01732.x

Moore, D., Robson, G. D., & Trinci, A. P. J. (2020). *21st century guidebook to fungi, 2nd edn*. Cambridge University Press.

Neville, P., & Poumarat, S. (2004). *Amaniteae. Amanita, Limacella & Trroendia (Fungi Europaei 9)*. Candusso Edizioni.

Oda, T., Tanaka, C., & Tsuda, M. (1999). Molecular phylogeny of Japanese *Amanita* species based on nucleotide sequences of the internal transcribed spacer region of nuclear ribosomal DNA. *Mycoscience*, *40*, 57–64. https://doi.org/10.1007/BF02465674

Rehner, S. A., & Buckley, E. (2005). A *Beauveria* phylogeny inferred from nuclear ITS and EF1-α sequences: evidence for cryptic diversification and links to *Cordyceps* teleomorphs. *Mycologia*, *97*, 84–98. https://doi.org/10.1080/15572536.2006.11832842

Ronquist, F., Teslenko, M., van der Mark, P., Ayres, D. L., Darling, A., Höhna, S., Larget, B., Liu, L., Suchard, M. A., & Huelsenbeck, J. P. (2012). MrBayes 3.2: Efficient Bayesian phylogenetic inference and model choice across a large model space. *Systematic Biology*, *61*, 539–542. https://doi.org/10.1093/sysbio/sys029

Ryberg, M. (2015). Molecular operational taxonomic units as approximations of species in the light of evolutionary models and empirical data from Fungi. *Molecular Ecology*, *24*, 5770–5777. https://doi.org/10.1111/mec.13444

Ryberg, M., & Matheny, P. B. (2012). Asynchronous origins of ectomycorrhizal clades of Agaricales. *Proceedings of the Royal Society B*, *279*, 2003–2011. https://doi.org/10.1098/rspb.2011.2428

Sánchez-Ramírez, S., Tulloss, R. E., Amalfi, M., & Moncalvo, J. M. (2015a). Palaeotropical origins, boreotropical distribution and increased rates of diversification in a clade of edible ectomycorrhizal mushrooms (*Amanita* section *Caesareae*). *Journal of Biogeography*, *42*, 351–363. https://doi.org/10.1111/jbi.12402

Sánchez-Ramírez, S., Tulloss, R. E., Guzmán-Dávalos, L., Cifuentes-Blanco, J., Valenzuela, R., Estrada-Torres, A., Ruán-Soto, F., Díaz-Moreno, R., Hernández-Rico, N., Torres-Gómez, M., León, H., & Moncalvo, J.-M. (2015b). In and out of refugia: historical patterns of diversity and demography in the North American Caesar's mushroom species complex. *Molecular Ecology*, *24*, 5938–5956. https://onlinelibrary.wiley.com/doi/epdf/10.1111/mec.13413

Shirai, M. (1905). *A list of Japanese fungi hitherto known*. Nihon-engei-kennkyukai.

Shirai, M., & Hennings, P. (1899). *Berlin-kinpu* (in Japanese), Hekisui Shirai.

Shirai, M., & Miyake, I. (1917). *A list of Japanese fungi hitherto known, 2nd edn*. Nihon-engei-kennkyukai.

Tedersoo, L., Jairus, T., Horton, B. M., Abarenkov, K., Suvi, T., Saar, I., & Kõljalg, U. (2008). Strong host preference of ectomycorrhizal fungi in a Tasmanian wet sclerophyll forest as revealed by DNA barcoding and taxon-specific primers. *New Phytologist*, *180*, 479–490. https://doi.org/10.1111/j.1469-8137.2008.02561.x

Trifinopoulos, J., Nguyen, L. T., Haeseler, A., & Minh, B. Q. (2016). W-IQ-TREE: a fast online phylogenetic tool for maximum likelihood analysis. *Nucleic Acids Research*, *44*, W232–W235. http://doi.org/10.1093/nar/gkw256

Tulloss, R. E., & Yang, Z. L. (2009). Notes on *Amanita* section *Caesareae*, *Torrendia*, and *Amarrendia* (Agaricales, Amanitaceae) with provisional division into stirpes

and annotated world key to species of the section. http://www.amanitaceae.org/content/uploaded/pdf/hemibkey.pdf

van der Linde, S., Suz, L. M., Orme, C. D. L., Cox, F., Andreae, H., Asi, E., Atkinson, B., Benham, S., Carroll, C., Cools, N., De Vos, B., Dietrich, H.-P., Eichhorn, J., Gehrmann, J., Grebenc, T., Gweon, H. S., Hansen, K., FJacob, F., Kristöfel, F., Lech, P., Manninger, M., Martin, J., Meesenburg, H., Merilä, P., Nicolas, M., Pavlenda, P., Rautio, P., Schaub, M., Schröck, H.-W., Seidling, W., Šrámek, V., Thimonier, A., Thomsen, I. M., Titeux, H., Vanguelova, E., Verstraeten, A., Vesterdal, L., Waldner, P., Wijk, S., Zhang, Y., Žlindra, D., & Bidartondo, M. I. (2018). Environment and host as large-scale controls of ectomycorrhizal fungi. *Nature*, *558*, 243–248. https://doi.org/10.1038/s41586-018-0189-9

Vassiljeva, L. N. (1950). Species novae fungorum. *Notulae Systematicae e Sectione Cryptogamica Instituti Botanici Nomeine V. L. Komarovii Academiae Scientificae USSR*, *6*, 188–200.

Vesterholt, J., Eberhardt, U., & Beker, H. J. (2014). Epitypification of *Hebeloma crustuliniforme*. *Mycological Progress*, *13*, 553–562. https://doi.org/10.1007/s11557-013-0938-y

Woodall, C. W., Oswalt, C. M., Westfall, J. A., Perry, C. H., Nelson, M. D., & Finley, A. O. (2009). An indicator of tree migration in forests of the eastern United States. *Forest Ecology and Management*, *257*, 1434–1444. https://doi.org/10.1016/j.foreco.2008.12.013.

Yamada, A., & Katsuya, K. (1995). Mycorrhizal association of isolates from sporocarps and ectomycorrhizas with *Pinus densiflora* seedlings. *Mycoscience*, *36*, 315–323. https://doi.org/10.1007/BF02268607

Yang, Z. L. (2005). *Amanitaceae. Flora fungorum sinicorum 27* [in Chinese]. Science Press.

Yasuda, A. (1920). Notes on fungi (95) [in Japanese]. *The Botanical Magazine*, *34*, 67–68.

Yoshino, M. (1986). *Climate in a small area*. Chijin-shokan.

Zhang, L. F., Yang, J. B., & Yang, Z. L. (2004). Molecular phylogeny of eastern Asian species of *Amanita* (Agaricales, Basidiomycota): taxonomic and biogeographic implications. *Fungal Diversity*, *17*, 219–238. http://www.fungaldiversity.org/fdp/sfdp/17-13.pdf

Zhang, R., Muller, G. M., Shi, X. F., & Liu, P. G. (2017). Two new species in the *Suillus spraguei* complex from China. *Mycologia*, *109*, 296–307. http://dx.doi.org/10.1080/00275514.2017.1305942